Master's thesis

NTNU
Norwegian University of Science and Technology
Faculty of Information Technology and Electrical Engineering
Department of Electric Power Engineering

Anders Ulfsnes

Investigating the Effect of Eccentric Conductor Positions on a Rogowski Coil in Laboratory and Finite Element Method Simulations

Master's thesis in Energy and Environmental Engineering
Supervisor: Irina Oleinikova
Co-supervisor: Mohammad Khalili Katoulaei, Hans Kristian Høidalen

June 2021

NTNU
Norwegian University of Science and Technology

Anders Ulfsnes

Investigating the Effect of Eccentric Conductor Positions on a Rogowski Coil in Laboratory and Finite Element Method Simulations

Master's thesis in Energy and Environmental Engineering
Supervisor: Irina Oleinikova
Co-supervisor: Mohammad Khalili Katoulaei, Hans Kristian Høidalen
June 2021

Norwegian University of Science and Technology
Faculty of Information Technology and Electrical Engineering
Department of Electric Power Engineering

NTNU
Norwegian University of
Science and Technology

Sammendrag

Endringer i strukturen til kraftsystemet gir nye muligheter og utfordringer for drift og vern av nettet. De siste årene har det kommet digitale nettstasjoner, men disse installasjonene skjer ikke over natten, og det kreves derfor nye flerteknologiløsninger. Rogowskispolen er en lovende strømsensor som har fordeler i verninstallasjoner. En stor fordel er at luftkjernen aldri mettes i motsetning til konvensjonelle strømtransformatorer med jernkjerne. Samtidig er det utfordringer som må løses. Den påvirkes av flere faktorer og i løsninger med differensialbeskyttelsesreléer kan dette forårsake uønskede feil.

Målenøyaktigheten til en rogowskispole testes i et laboratorieoppsett. Posisjonen på lederen endres for å undersøke hvordan dette påvirker utputten. Resultatene viser ingen åpenbare trender i utputten når lederposisjonen endres, men generelt endres feilen når lederen flyttes bort fra sentrum. Feilen til rogowskispolen som testes er generelt ganske høy med hele $1,6\%$ feil i sentrert posisjon. Feilen endres deretter med opptil $0,25$ prosentpoeng når lederen flyttes ut fra sentrum.

En modell lages med endelige elementers metode for en rogowskispole og konfigureres til å etterligne den som ble brukt i eksperimentet. Modellen lages i 3D i en flerfysikksplattform. Modellen testes i ulike konfigurasjoner og parametere. Først har spolen 16 viklinger, og feilen som måles i forhold til den sentrerte lederposisjonen er mye høyere enn de som ble målt i laboratoriet. Feilene viser også trender i hvordan lederposisjonen påvirker feilen. For å forsøke å gjenskape resultatene fra eksperimentet blir det forsøkt å gjøre viklingstettheten mer tilfeldig, slik at den i større grad kan gjenspeile hvordan viklingene blir laget i virkeligheten. Resultatene blir noe endret, men etterligner ikke resultatene fra eksperimentene i særlig grad. Antall viklinger blir så økt til 48 og testene repeteres. De resulterende feilene er nå cirka like store som de som ble målt i laboratoriet.

Laboratorieoppsettet har flere begrensninger som bør fikses. Deretter kan forbedrede tester brukes til å verifisere modellen. Bruken av en endelige elementers metode-modell er en verdifull metode for å forske på rogowskispolen ettersom man enkelt kan undersøke ikkeideelle konfigurasjoner. Modellen kan også utvides med en integrator og kompenseringsteknikker. Dette gir flere muligheter for å utvikle løsninger som gjør at rogowskispolen en brukbar sensor i flerteknologiløsninger i vern og for pålitelig operasjon av systembeskyttelsesløsninger.

Abstract

Changes in the power system structure create new possibilities and challenges in the protection and operation of the grid. Digital substations are emerging, but these installations are not done overnight, and hence the transitions require new thinking in terms of interoperability in protection applications. The Rogowski coil (RC) is a current sensor which offers benefits in protection schemes. Preeminently that the air core does not saturate, compared to conventional iron core Current transformers (CTs). But challenges limit its current applications. It is affected by several influencing quantities and in differential protection schemes this can cause malfunctioning.

A test rig is developed, and the measurement accuracy of a RC is tested in the setup. The conductor position is adjusted to investigate the effect on the output. The overall accuracy is about 1.6% error in the centered position. The accuracy changes up to 0.25 percentage points with the eccentric configuration. The RC output varies based on where the conductor is located, but trends in how conductor adjustments affect the error is not obvious.

A Finite element method (FEM) model is created for a RC configuration similar to the one used in laboratory tests. The model is created using 3D geometry in a multiphysics environment. The model is tested with several configurations and parameter changes. Initial tests with 16 turns result in composite errors with a magnitude which is a lot higher than what is achieved in the laboratory tests. To investigate how randomness in the winding distribution affects the output, an inhomogeneous winding distribution is used. The resulting output is only slightly changed compared to the homogeneous test. With 48 homogeneously distributed turns the error resembles the values achieved in the lab, but with clear patterns related to how the conductor adjustments affects the error.

The laboratory setup has several limitations which should be improved. It can then be used to verify the FEM model. Using a FEM model is a valuable method of researching the RC as it can assess nonideal configurations. It can also be extended to utilize an integrator and compensation techniques which can be designed to improve the accuracy. This can make the RC a viable current transducer in interoperable protection applications and reliable System protection scheme (SPS) operation.

Preface

The author wants to thank PhD candidate Mohammad Khalili Katoulaei who helped a lot with the organization of the laboratory tests as well as inputs and help with the simulation model. Mr Katoulaei has been very helpful and available at most hours during the week. Thanks to supervisor professor Irina Oleinikova for guidance and follow ups during the process of the master thesis, for inputs on the structure and contents in the thesis and for feedback on the work conducted. Thanks to Aksel Andreas Reitan Hanssen for generous support and logistics help related to obtaining devices for use in the laboratory work. Thanks to Anders Gytri for IT support related to server and desktop simulations.

The work leading up to the thesis has spanned one year. The first part of the work focused on preliminary literature studies, and basic modeling of RCs using lumped parameters. The second part goes further into the performance of the RC. Materials from the first part of the work is reused in the thesis as it gives a background in the uses of the RC in protection applications ans system protection schemes. These parts are: chapter 1 including *Trends in the Power System*, chapter 2 including *System Protection Schemes* and *Differential Protection*, as well as the introduction to chapter 3 and its first section *Modeling & Output Integration*.

Table of Contents

List of Tables

List of Figures

List of Abbreviations

ANN Artificial neural network

CB Circuit breaker

CT Current transformer

DSP Digital signal processing

FACTS Flexible alternating current transmission system

FEM Finite element method

GOOSE Generic object oriented substation events

GPS Global positioning system

HVDC High voltage direct current

IED Infinite element domain

IoT Internet of Things

MAC Media access control

MU Merging unit

NCIT Nonconventional instrument transformer

OpAmp Operational amplifier

ppm Parts per million

PT Potential transformer

PV Photovoltaic

RC Rogowski coil

SPS System protection scheme

SV Sampled value

UFLS Under frequency load shedding

VT Voltage transformer

WAMS Wide-area measurement system

WP4 Work package 4

Chapter 1

Introduction

As the global effort for the climate change increases, so does the demand for cleaner energy production. Penetration of renewable energy sources introduces more power electronics equipment in the power system. Distributed power generation from these renewables causes a change from the traditional power system. These changes contributes to possibilities and challenges which must be overcome to protect the integrity, reliability and utilization of the power system.

The traditional power system has large centralized power generators, and demands at other locations, usually in industrial, commercial and residential areas. Hence, the power flows from the generators to the consumers. The generators and loads are connected through the transmission system and distribution systems. As voltage levels vary from generation to the end customer, transformation is needed. This is done at substations. Here, multiple lines are connected through busbars, acting as a connection point between different lines. The substations contains transformers for transforming voltages between the levels of the interconnected lines. Additionally, switches, monitoring and protection & control equipment are installed at these substations. Instrument transformers are used to measure voltages, currents and power in substations.

Different strategies are used to protect the power system from faults. Relays can be used to protect lines, busbars, transformers and generators. These relays are area protection devices which protects a certain element, for example a transformer, line or busbar, from damages if a fault happens. Failure to do so might also cause serious danger for the surroundings [1]. In substations, relays are installed in selectivity setups which is designed

such that protective action should affect the system as little as possible. Less selective protection acts as a backup service if the primary protection relay did not take appropriate action to clear the fault. Hence, these have intended time delay causing them to operate slower than the primary protection [2]. The relays utilize current and voltage transducer to pick up changes in the power flow. Traditional differential protection schemes relies on two conventional CTs and triggers if they measure different current levels.

1.1 Trends in the Power System

Industry 4.0 has set the path for digitization of the power system [3]. Such power systems are denoted smart grids. The change from traditional power systems to smart grids have different aspects. Benefiting from digitization, the smart grids utilizes Internet of Things (IoT) equipment so that every component in the power system can communicate. This enables data handling from different sources, that provides a cohesive and integrated view of the system being measured. Similarly, solutions are supported to increase situational awareness, and selection of optimal control actions to manage bottlenecks or disturbances. Furthermore, as power electronics equipment is getting cheaper and manageable, such systems are installed in the power system to increase utilization, manage advanced electric machines and for dynamic control of scenarios. Flexible alternating current transmission system (FACTS) equipment are examples on power electronics equipment used to control the power system. International connections, and offshore power generation is also growing, which introduces the need for High voltage direct current (HVDC) transmission systems. These are able to transfer power over long distances with lower losses than traditional AC systems. These transmission systems requires a lot of power electronics equipment. Power electronics equipment reduces the voltage quality and could lead to decreased stability limits [4]. Lastly, renewable energy production like wind and Photovoltaic (PV) generation is altering how the transmission of power is flowing. Unlike the traditional power system, smart grids have distributed power generation which means power generation can happen in the industrial, commercial and residential areas as well. The power system structure transitions from the traditional power system to smart grids is shown in figure 1.1. From these changes arises endless possibilities for improving the power system. This comes at a cost: The distributed generation, power electronics equipment, and introduction of new power generation creates challenges which has to be overcome.

As investments in renewable power generation grows, the net generation in the power system often increases. Especially in countries like Norway, renewable power production is installed to supply other countries instead of decommissioning carbon based production units. If new transmission lines are not installed, the stress on the power system increases.

More renewable production and HVDC links are being installed in the Norwegian grid [5, p.12]. These have low inertia, which means a change in load will cause a large change in frequency. Synchronous machine connected hydro plants have high inertia and governor control which causes high damping of disturbances, giving stable protection against tripping of lines. Such systems are easier to control. Wind farms with low inertia, has low damping, and such disturbances will hence tend so oscillate, and give large frequency changes [5, pp.35-41]. In future power systems close to the shore, with offshore wind farms and international grid connections, the low total inertia can cause frequency challenges. In interconnected power systems the effects of disturbances and faults can have

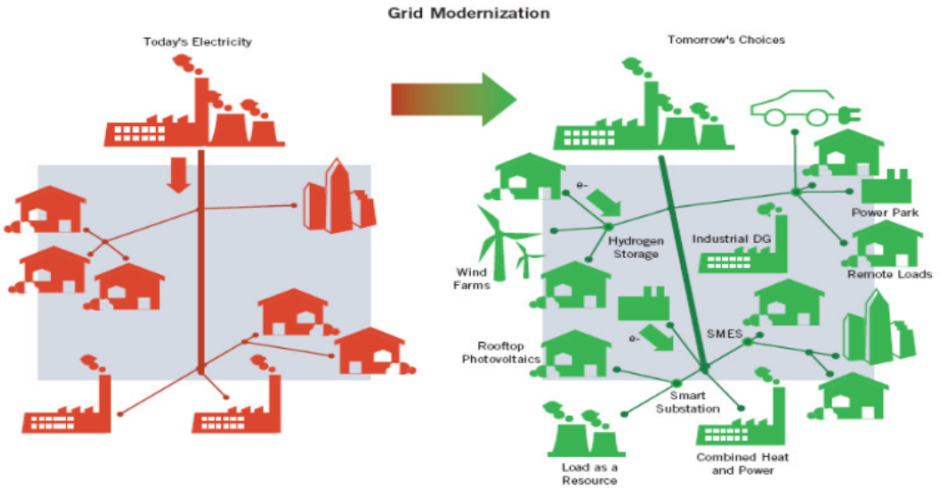

Figure 1.1: The traditional grid compared to IEEE's vision of the smart grid structure [6].

impacts on the rest of the network far from the location where the disturbance or fault happened. For example, in 2003 trees short circuited a 345 kV line in Ohio, and as a result multiple lines and generators disconnected in the area in order to protect equipment. This caused a cascading effect, and ended in the blackout in the power system affecting 50 million people in Northeast USA and Ontario, Canada [7]. A local fault hence affected a great part of the power system. To prevent this, trimming of the trees could be done. However, even if safety precautions can be done, the risk of faults is always present. Some other examples on blackouts are Ukraine 2015, Venezuela 2019 [8], and India 2012 [9]. In such cases, the area protecting devices are not sufficient for protecting the power system. SPSs were designed to protect bigger areas of the power system, utilizing special control schemes for protecting parts of the system from wide area faults.

The protection of the power system relies on transducers. Without these, the state of the system is unknown, and actions for controlling or protection the system is impossible.

Measurement systems operating quickly are necessary for determining appropriate action in protecting the system upon a fault. Industry 4.0 and the digization of the substations allows for new digial sensoring technology, and protection schemes. Fast communication solutions interconnect equipment and substations, but the performance of these communications are dependent on latency, jitter, redundancy and cyber security [2].

1.2 Scope of Thesis

Digital substations offer benefits for the design of SPS. In the traditional substations, the complexity of cabling in connections made advanced protection systems hard to implement, but the new digital substations offers endless possibilities for configurations. Internet communication means no new cables must be installed for a new protection algorithm to be implemented.

The reliability of these schemes are dependant on transducers, which motivates the research on the RC for use in differential protection schemes in digital substations. Traditional substations utilize CTs, but the use of these is not without challenge. The iron cores means they are difficult to install in cramped locations, and they become costly when designed to operate without saturation during faults [10]. Hence, saturation of CTs is possible in practical installations. Saturation of CTs can cause maloperation of protection relays [11, 12, 13]. In worst case scenarios CT maloperation can cause cascading wide effect faults. The research on RCs have therefore gained interest in the last years [14, 15, 16, 17, 18, 19]. The preeminent benefit is that the lack of an iron core means it does not saturate. The air core make it a cheaper option than the conventional CT. There are however, some challenges that most be overcome before the RC can be the primary option for protection applications transducers. Compared to the CT the RC is more prone to influencing quantities like conductor position, conductor angle, temperature and frequency deviations [20, 21, 22]. This influences affects the measurement accuracy, and this can result in malfunctioning of relays in protection applications. The RC is discussed more in-depth in chapter 3.

The background for this thesis is to advance the research on the RC for protection applications. Several proposed methods of RC modeling exists. The lumped model, the distributed model and numerical models have primarily been utilized [23, 24, 25]. FEM models allow for more complex modeling compared to these methods. RC FEM modeling have been conducted in several publications [26, 27, 28]. The design of a FEM model is a powerful and realistic method for simulations which can be used to lay the groundwork for further work on the RC. Influencing quantities can be difficult to avoid, but if these quanti-

ties can be sensed using external sensors, then the measurements can be compensated and the measurement accuracy of the RC is assured in all operation situations. This in turn can ensure safe operation of the power grid during faults, and defend against wide area faults in the future.

The goal of the work is to test the accuracy of a RC in an appropriate test rig and build a FEM model to simulate the RC. This model is to work as a basis for the future development of compensating techniques. Compensating techniques utilizes sensors to obtain parameter changes in the RC configuration, and applies digital compensation of the signal to increase the accuracy. For example by using hall effect sensors to determine the conductor position. The model can be used to investigate how different parameters influence the signal, and to determine valid compensating techniques. The possibilities for such a FEM model are endless, at the cost of computational power. Because of the geometry of the RC 3D models must be used, which quickly increases the complexity of these simulations compared to the 2D counterparts. Such models are however valuable as it offers benefits for future research into the topic. The research on protection applications can benefit from this work because a compensated RC might be able to work interoperable with a conventional CT in a differential scheme. This benefits the digital substations as upgrades can be done gradually.

The objectives of this thesis are the following:

- Develop a laboratory setup for testing the accuracy of a RC
- Test the influence of conductor positions on the RC in the laboratory environment
- Create an 3D FEM model of a RC
- Simulate conductor position changes and evaluate the effects compared to the laboratory tests
- Contribute to developments in RC modeling and accuracy compensation techniques using FEM model
- Contribute to protection applications interoperability research
- Contribute to the use of the RC in reliable SPS operation

Chapter 2

Power System Protection

As digital solutions are incorporated into the power system, new protection possibilities appear. The role of protection in the power system is to secure the reliability of power transmission. Reliable electricity supply is becoming increasingly important for the society, and pressures on the utilization of the power system is pushed as economic powers and renewable power generation increases [29]. System protection schemes, and digital substations offers possibilities to deal with these challenges.

The traditional substations lacks smart systems for communication in the substation. In the control building data from the substation can be sent to the power system operator. Communication within the substation consists of hardwired analog signals from CTs, Voltage transformers (VTs) and Potential transformers (PTs) to relays. The relay output are then transmitted analogous to Circuit breakers (CBs) and other relays [30]. For this communication to work, a lot of hardwired cabling is needed, because a one wire must be installed between each communicating device. Additionally a wire must be run to the control house for monitoring. Configurations, repair and installment of equipment in such substations require a lot of effort. These analogous wires requires specific sizes and length for the accuracy of measurements, and additionally these can cause safety issues for personnel or equipment [31].

The introduction of digital substations enforces communication inside the substation on a peer to peer basis. This is assured by the process bus. The process bus is an Ethernet based communication channel between process level switching devices and bay level intelligent electric devices for protection and control applications [32]. Whereas in traditional sub-

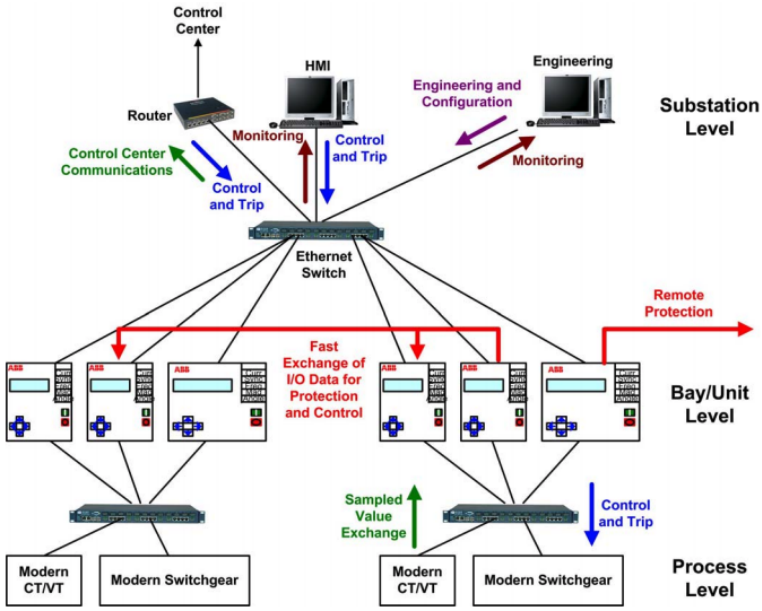

Figure 2.1: An overview of an IEC 61850 based substation [37].

stations, signals were sent as analog electrical signals, the process bus transmits digital signals. Smart technology for sending and receiving data is installed on the process bus which allows uncongested data communication on the process bus. An apparent advantage of this is that the need for excessive cabling is reduced as all signals can be transferred through one or a few process busses. Additionally, control and measurements is electrically disconnected from the HV side of the substation, which decreases risk of injury [33]. Digital substations require time synchronization for all digital signals. This is usually done using a Global positioning system (GPS) satellite clocks. The clock signals are added to signals and measurements. Global synchronization is an requirement in Wide-area measurement system (WAMS) [34]. In order to utilize the benefits of the digital substation, the sophisticated communication of the process bus is required. In turn, this communication needs a robust communication standard. The solution is IEC 61850.

The IEC 61850 standard is made especially for substation automation. The project was started in during the 90s and was originally a cooperation between the US and EU (UCA and IEC) [35]. As corporations was growing more international a demand for standardized communication was growing. Units from numerous different providers meant it was troublesome to add functionality to the power system. The main goals of the standard is to give interoperability, free configuration and long term stability [36]. IEC 61850 sets rules for communication between intelligent electric devices in digital substations. IEC 61850

based digital substations employ the process bus for communication between devices. The process bus needs clear rules for transmission in order to work. Otherwise, packets would interfere and congest, and intelligent electric devices of different vendors will not be able to communicate. The benefits of IEC 61850 are [38]:

- Reduce dependence on multiple protocols
- Reduce construction cost by eliminating most copper wiring
- Automate substations
- Real time distributed computing
- Advanced management capability
- High speed peer to peer communications
- Improved security/integrity
- Flexible programmable protection schemes and ease of maintainability

A schematic of an example IEC 61850 based digital substation is shown in figure 2.1. Switches between Infinite element domains (IEDs) on the process level facilitate support for peer-to-peer communication. Centralized control and monitoring can be done both at the substation, and in a control center at a different location. Configuration and installation of new equipment is easy, as all IEDs can be reconfigurated from a central unit through the switches. Peer-to-peer communication between units means transmission of data has greater performance, compared to the traditional setup where signals had to go through a central unit. IEC 61850 also includes support for multitechnology communication, which means relays are able to communicate directly with CTs, VTs and switchgear.

Generic object oriented substation events (GOOSE) is a functionality introduced with IEC 61850. GOOSE communication can happen on a peer-to-peer basis. This means the IED can communicate automatically between each other which significantly decreases the transfer time compared to a system where messages have to go through a central unit. This allows for quick circuit breaker action upon a relay trip in a substation. The GOOSE service is based on Ethernet multicast transmission which provides fast, efficient and reliable communication between the nodes [39]. Multicast addresses are addresses which multiple devices respond to. Hence an intelligent electric device only has to transmit one message to communicate with all subscribing intelligent electric devices. This design eliminates

the need for TCP/IP protocols, which reduces the complexity and time of transmission. Additionally, the use of a GOOSE based process bus means a number of virtual ports can be utilized in an intelligent electric device which has limited input and output ports [40]. As the name implies GOOSE are object oriented messages. The benefit of this approach is

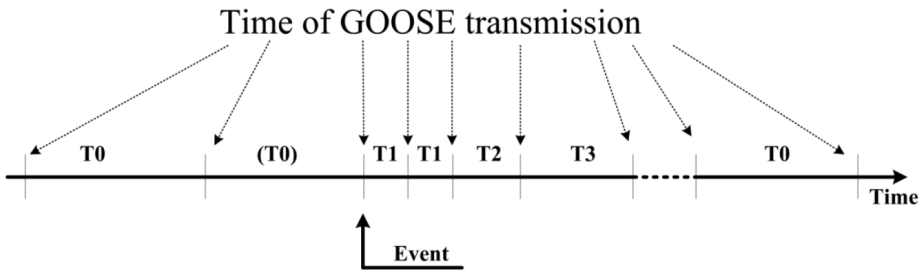

Figure 2.2: Normal condition (T_0) and heartbeat messages (T_1, T_2, T_3) for GOOSE packet transmission [32].

that all kinds of data can be transferred using the same protocol whether it is fault data, trip signals or breaker status.The functionality for different data types is what makes GOOSE object oriented, and offers great benefit for event messaging. For this to work, all IEDs in a substation must be configured to handle the type of data being transmitted. Depending on the setup in the substation, different types of data can be transmitted, sending only what is necessary. This reduces the size of GOOSE packages. GOOSE messages are sent out rapid intervals when an event happens in a substation. The transmission will be resent at a given frequency, which will be lowered until the maximum heartbeat frequency is reached. After this, events are transmitted at a fixed, slower frequency. This mechanism is called heartbeat messaging, and enables fast transmission of events, and slower constant updates during normal conditions. figure 2.2 shows this method of transmitting event data.

IEC 61850-9-2 set the rules for Sampled value (SV) in digital substations. SV are used in for sending and receiving of current and voltage measurements on the process bus. In order to reduce the overhead of communication on the process bus, SV is directly mapped to the link layer under Ethernet type *88 ba* [39]. SV packets are created in Merging units (MUs), which digitizes current and voltage measurements, and time stamps the packets with a time stamp from the digital substation synchronization unit. The Ethernet protocol supplies destination and source Media access control (MAC)-addresses for where the SV is sent and received. Like the GOOSE protocol, SV also uses multicast MAC-addresses which means packets of both protocols can be transmitted on the process bus.

2.1 System Protection Schemes

SPS are defense plans against cascading effects in the power system. If such a fault happens, the SPS will act and control the cascading effect - avoiding a potential blackout. [41] argues that as complexity of network operation increases, because of growth in load, changes in market conditions and increased import and export. The network becomes more stressed, and hence SPS are growing in popularity. In power systems with low inertia it is harder to maintain frequency stability, which increases the risk of blackouts. The commissioning of new renewable power production decreases the overall inertia of the system [42]. This further emphasizes the importance of SPSs.

Generally SPS can be categorized as controllers having the following properties [43]:

- SPS can be armed or disarmed depending on system conditions
- SPS are "normally dormant" systems; initiating events usually occur less than once a year
- SPS usually employ discrete, feed forward control laws
- The control action taken is predetermined in most cases
- Typically some form of communication is involved in the control action

Even though the SPS systems are not often used, the blackouts exampled in section 1.1 shows the importance of these systems. These schemes can exist in different forms, with diverse goals. [44] presents these types of SPS:

- Generation rejection
- Load rejection
- System separation
- Turbine valve control
- Load and generator rejection
- Out-of-step relaying
- Discrete excitation controls
- Dynamic breaking
- Generator runback
- VAR compensation
- Combination of schemes

In the Hydro-Quebec area automatic measures are conducted upon predetermined events. Switching of 735 kV shunt reactors to stabilize voltage levels done under extreme contingencies, generation rejection and load shedding done upon losing multiple 735 kV lines.

Underfrequency load shedding is performed to balance load and generation, and under-voltage load shedding is being studied [45]. Such SPS are usually triggered by a change in frequency or voltage. Depending on how much it changed, generation or load is tripped. This is done to balance the system, and hence assure voltage and frequency stability. SPS can be simple in nature, operating in a local area, or they can be wide area based. A survey on the SPS was conducted in [45]. Here it was found that many of the existing SPS were based on local data. The local SPS can be simple and effective, but wide area protection offers a more reliable protection as measures for protecting the network is coordinated. In the example given on the 2003 blackout, the cascading effect in the network started the blackout. A local SPS could perhaps reduce the cascading effect when it reached the area. However, if a wide area coordination SPS was implemented, the cascading effect would never start. Such schemes requires sophisticated communication between areas and inside substations. Traditionally such communication does not exist in substations. A system protection terminal is shown in figure 2.3. This presents a general overview on functional-

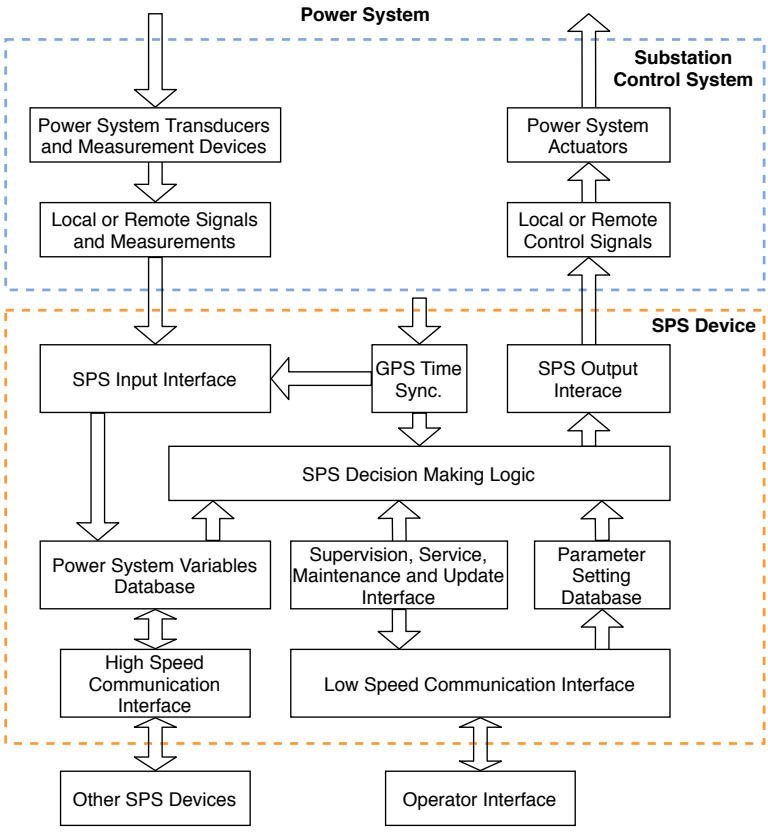

Figure 2.3: A system protection terminal [45].

ities of the SPS and interfaces to other SPS, the operator, measurements and actuators. The figure indicates that two concepts are of importance for the operation of SPS. Firstly, high speed communication between devices are needed to assure that the schemes can operate quickly enough when a fault happens. Secondly, power system transducers and measurement devices must be used to perceive such events. In a system of different vendors, and hardwired centralized communication, such schemes are not effortlessly implemented, as a lot of new cabling most be done.

In systems with multiple SPSs [43] found that inadvertent interactions between SPS could be catastrophic. From a process view the schemes seemed satisfactory, but when looking from a system point of view, the negative interactions between SPSs caused challenges. In North America, it was found that in 70% of major blackouts relays contributed to the initiation or evolution of the blackouts [46]. [47] states that zone 3 distance protection relays misoperation has a major contribution to enforcing cascading effects. Zone 3 distance relays are backup protection devices which protects larger sections of transmission lines. Hence, the need for smart relays, and system wide protection schemes are of importance in order to protect the power system, and to hinder the inadvertent interactions of SPSs.

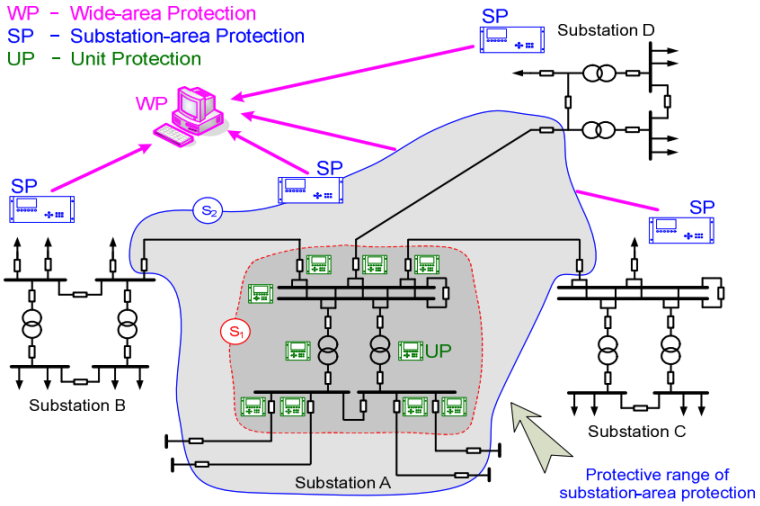

Figure 2.4: A novel protection architecture in smart grids [48].

Some novel SPS takes advantage of WAMSs and uses this to trigger minimal intruding actions which stabilizes a wider area of the power system. Such schemes require inter-substation operation, and as such, relies on smart communication technology which is reliable, fast, and secure. With existing communication solutions for digital substations, the cost of interconnecting the communication over wider areas is insignificant [35]. Traditional measurement systems uses local clocks for time stamping measurements, which

causes a challenge in calculating the exact system states [49]. To overcome this, novel SPS utilizes GPS synchronized time stamps. A novel protection architecture is shown in figure 2.4. In such a system, the protection of a substation is differentiated into areas. Unit protection happens at a local area, with local measurements. The substation protection measures faults inside the substation, and operates as a redundant primary protection when unit protection equipment is out of service. Further, the substation protection should work as an optimized backup protection which operates when the unit protection maloperates. The wide area protection lastly uses WAMS, and cooperates with other substations to make decisions based on potential wide area disturbances [48]. This system should accordingly be able to protect against faults during normal conditions and during maloperation, and stop cascading effects in the power system.

The use of novel technologies and approaches in SPS have been implemented and proposed. [50] uses a WAMS based Under frequency load shedding (UFLS) algorithm with promising results compared to conventional schemes. Artificial neural network (ANN) based UFLS schemes have also been proposed. [51, 52] used such algorithms for a SPS in a isolated system. These schemes are fast, robust and gives optimal load shedding values. A drawback of ANN-based UFLS schemes is that they have to be trained on known data, and will hence have trouble with unknown cases [53].

As the power system increases in complexity, the need for SPS increases. In order to protect against wide area disturbances, smarter schemes are required. Computational intelligence techniques can reduce the risk of blackouts [54]. WAMS have the potential for advancing SPS and its operation performance [44]. Sophisticated communication technologies, IEDs and inter-substation cooperation is however required in order to take advantage of these solutions.

2.2 Differential Protection

For protecting components in a power system, or switching out areas from faults, relays are used. These are protection equipment which uses electromechanical, static, digital or numerical technologies which triggers protective measures when a faulty event occurs [55]. The relays are dependant on transducer measurements. These measurements are read in the relay, and based on the technology used, an analog or digital trip signal is outputted if the measurements indicate that a fault has happened. Earlier, electromechanical relays were often used. These uses coils or temperature expanding metals to create mechanical forces with operates a relay contact. Although the electromechanical relays still exist today, more modern technologies are rapidly introduced, especially in high voltage power

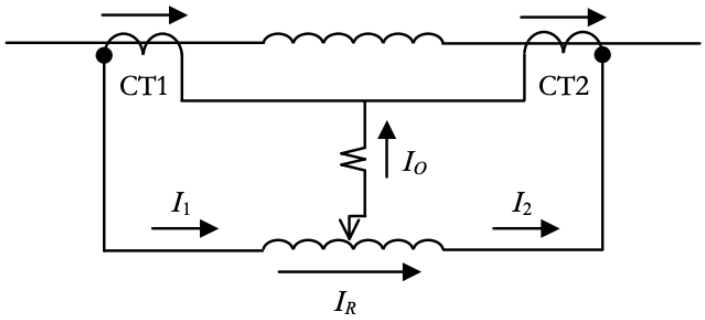

Figure 2.5: Differential relay connection diagram [57].

systems [56] Digital relays depends on digitized measurements. These are then compared in a logic algorithm which based on the measurements outputs a boolean value which a CB acts on. An inherant benefit of digital relays is that different types of relay schemes can be configured. Examples of relay schemes are differential relays, differential relays and overcurrent relays. An electromechanical relay on the other hand, is designed to feature just one such scheme.

Differential protection is used to protect one or more components in between a protected zone. Current measurements from both sides, I_1 and I_2 are compared. Hence this relay demands that CTs are chosen appropriately. A differential protection scheme is shown in figure 2.5. In this figure the topmost inductor is the protected unit. Two CTs is situated on both sides of the protected unit.

Equation (2.1) is an expression of the differential current, denoted as I_0 in figure 2.5 in relation to the transformed currents.

$$i_d = i_{1s} - i_{2s} \tag{2.1}$$

$$i_r = \frac{i_{1s} + i_{2s}}{2} \tag{2.2}$$

$$i_d \geq K i_r \tag{2.3}$$

In equation (2.1) i_d is the differential current, i_{1s} is the transformed current from CT1 in figure 2.5. i_{2s} is the transformed current from CT2. A restraining current is used to make a comparison for the differential current. It is the average of the transformed currents. The restraining current is given by equation (2.2).
The percentage ratio, K, is typically set between 10-40% [56]. K can hence be set according to the level of sensitivity wanted. It should cover measurement errors, ratio mis-

matches, margins and more. Additionally tap changing transformers must be accounted for when using such relays. Level detection is implemented when designing relays. These are configured by the pickup setting which is the minimal current where the relay will trip. Figure 2.6 shows this effect. In order to trip this relay, a minimum current, 1.0 pu in the figure, and a minimal time is necessary to operate the relay. Interoperability of differen-

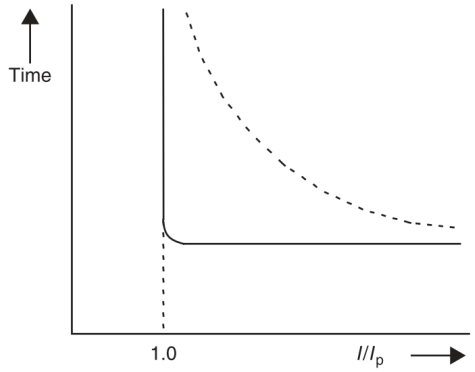

Figure 2.6: Characteristics of a level detector indicating pickup settings in relays. A minimal current and time is necessary to initiate a trip [56].

tial protection schemes poses challenges as equation (2.1) should net close to zero when in normal conditions. If the measurement have phase shift or magnitude differences, the differential current can be quite high even at normal conditions. The pickup setting should be configured to encompass this. Small disturbances, and external faults should not trip the relay, and must hence be considered as well. Conventional CT saturation could cause undesirable tripping of relays.

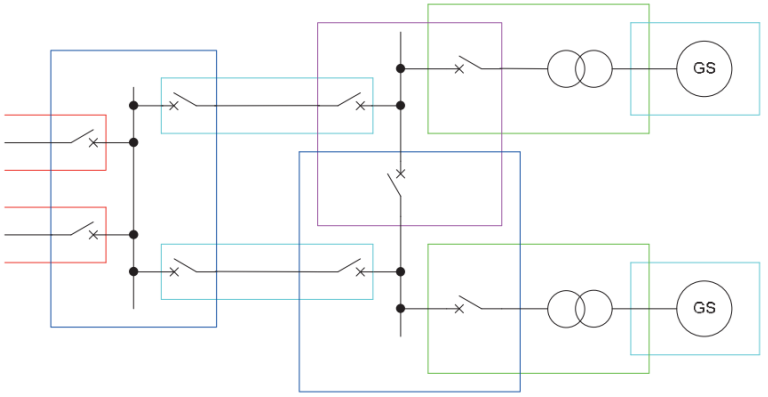

Figure 2.7: Overlapping protection zones denoted with different colors in a power system [55].

In SPS lots of relays are necessary to operate protective action over a wider area. In power

systems, relays are located such that the necessary units are protected. Additionally, to protect against maloperation of relays, backup relays are placed with a delay of operation such that these can protect the units of the primary relay failed. Protection areas are hence places such that protective schemes overlap each other. An example of this is shown in figure 2.7.

In conventional differential unit protection schemes, and as shown in figure 2.5, two conventional CTs are used to measure currents used in the relay operation. However, as Nonconventional instrument transformers (NCITs) are growing in popularity solutions for interoperable cooperation between CT and NCIT is of interest. Since differential protection relies on equal measurements on both sides of the unit, such configurations could cause challenges as measurement accuracy, saturation, bandwidth, and phase shift could cause a non-zero differential current during external faults, steady state or disturbances in the grid.

2.3 Prodig Perspective on Digital Substations

The ProDig project is a research project. It is a cooperating between the Electrical Power Engineering and Information Security and Communication Technology departments at NTNU, UiO department of Technology Systems, SINTEF Energy Research and Michigan Technological University. Information on the project is found on the official website [58]. The project focuses on power system protection and control in digital substations. Four PhD students and one PostDoc work on different aspects of digital substations and are organized into seven work packages. This thesis correlates with Work package 4 (WP4) which focuses on the use of NCIT and sensors in protection applications. The use of NCITs in differential protection interoperability configurations with conventional CTs is a research topic of interest.

The ProDig utilizes real time simulators, relay test devices, IEDs, process buses and satellite clocks to emulate a digital substation centered at the NTNU relay laboratory. This configuration, seen in figure 2.8, allows for practical tests of communication techniques, interoperability setups and use NCITs sensors. Parts of the goal is to investigate the interoperability of different sensors in a differential protection scheme utilizing IEC 61850 based process buses with GOOSE and SV communication. In order to use the RC in an interoperability configuration with CTs, initial research into the topic of RC is required.

One of the focus areas of WP4 is to utilize sensors to determine compensating signals to correct a measurement if the transducer deviates from the standard condition. One

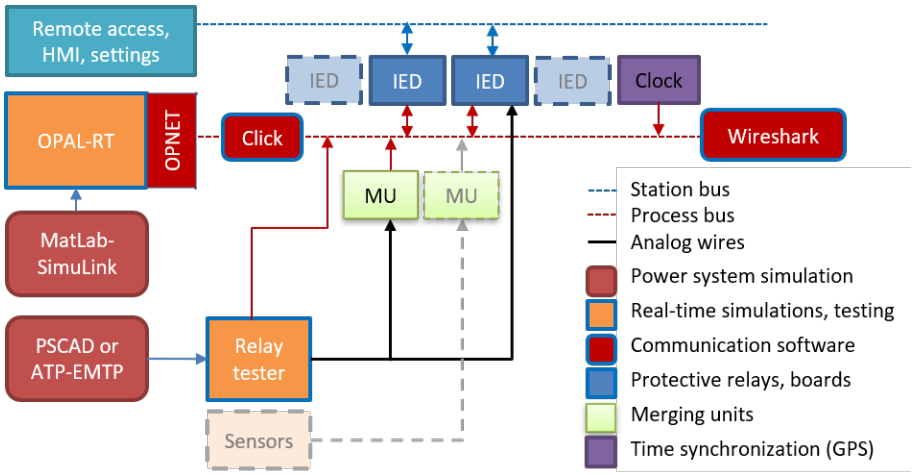

Figure 2.8: Schematic of technology used and intended interconnection of communication withing ProDig project laboratory resources [58].

example is to use hall effect sensors to determine the conductor position, and based on this apply compensation through the RC integrator. The accuracy testing laboratory setup designed for this work can benefit the project through the thesis and future tests performed by ProDig associates. This thesis contributes to the research project by creating data to work with and a model which can be developed with these compensating techniques. The project can use these results to do further testing in a mixed technology setup with a RC and a CT in a differential protection scheme using the ProDig laboratory.

Chapter 3

Rogowski Coil Modeling & Testing

The Rogowski coil (RC) is a NCIT, and was proposed in 1912 by W. Rogowski and W. Tannhaus [59]. At the time the limited amplitude of the output meant it had confined applications [20]. However, in recent years the RC has received new interest as the methods of creating the coil, and analyzing the output through Digital signal processing (DSP) has improved. Hence, making it a viable option in IEC 61850 based digital substations. The main benefits of the RC are the following [23]:

- Enduring large overloads without damage
- Measuring current in an extensive range, without saturation
- Easy to use, due to flexibility and light weight
- Low cost
- Non-intrusive nature (drawing no power from the main circuit)
- Wide bandwidth, in a range of 0.1 Hz to 1 GHz
- Excellent transient response
- Safety (isolated from the main circuit, electrically)

A RC is shown in figure 3.1a. The conductor in the figure is the conductor for which the current is measured. Here, $v_{out}(t)$ is the output signal of the coil. The lack of an iron core compared to conventional CTs gives the RC linear properties without saturation. Figure 3.1b shows a proposed solutions where the high current bandwidth and the non-saturation nature of the RC means one RC can replace multiple CTs in protection and metering applications as a current sensor or multi-purpose sensor.

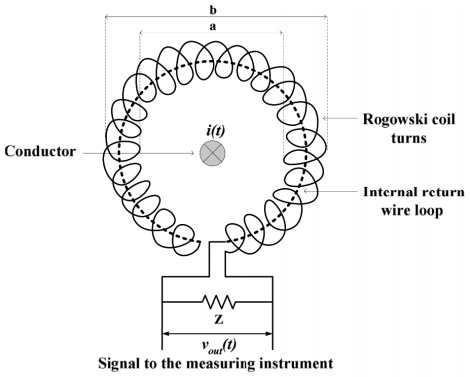

(a) A RC structure. Here shown with an internal return wire loop [60].

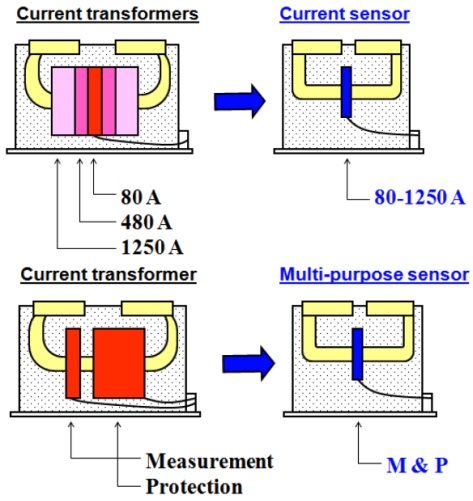

(b) Proposed solution where one RC can replace multiple CTs in metering and protection applications [61].

In conventional CTs the open circuit voltage can be up to 10 kV. As the RC lacks an iron core, there is weak coupling between the primary and secondary side so a maximum voltage up to about 10 V will be applied to the secondary side even during faults. This makes the RC safe to operate, and removes the instrument security factor requirement [61].

3.1 Modeling & Output Integration

For a toroidal with an enclosed loop ampères law is given as

$$\oint_C \mathbf{B} \cdot d\mathbf{l} = \mu_0 \int_S \mathbf{J} \cdot d\mathbf{S}. \tag{3.1}$$

B is the flux density, $d\mathbf{l}$ is a line element along the curvature of the coil denoted as the dotted line in figure 3.1a, **J** is the current density in the conductor and $d\mathbf{S}$ is an area element, where S is the area inside the coil. When a conductor is entrapped in the coil, the right side of equation (3.1) equals the total current flowing through the torus center. This results in

$$i(t) = \frac{1}{\mu_0} \oint_C \mathbf{B} \cdot d\mathbf{l} \tag{3.2}$$

Further, as **B** and **l** is parallel in all locations along the torus, and $\mathbf{B}(t)$ varies with time only, the following relation can be found

$$\mathbf{B}(t) = \frac{\mu_0 i(t)}{2\pi r} \tag{3.3}$$

where r is the radius to the center of the torus. In figure 3.1a, this is

$$r = a + \frac{b-a}{2}$$

Faradays law can be expressed as

$$v_{out}(t) = -\frac{d\phi}{dt} \tag{3.4}$$

The sign of equation (3.4) can be ignored. Assume that the torus has N windings along the torus axis. The change in total flux, ϕ is then given by the rate of change of the total flux density through all the windings in the torus as expressed in equation (3.5). Equation (3.3) is used to relate flux to the current.

$$\frac{d\phi}{dt} = \int \dot{\mathbf{B}(t)} \cdot d\mathbf{S} = A_w \dot{\mathbf{B}(t)} = \frac{\mu_0 \dot{i(t)}}{2\pi r} \tag{3.5}$$

here $d\mathbf{A}$ is a area element in the winding, and A_w is the area of a winding which is assumed to be constant when a RC is created with solid materials. Now, by combining equation (3.4) and equation (3.5), the current in the conductor can be expressed as

$$i(t) = \frac{2\pi r}{\mu_0 A_w} \int v_{out}(t) dt \tag{3.6}$$

The constant coefficiant can be expressed as the sensitivity or mutual inductance, M of the measurement, and hence equation (3.6) becomes

$$i(t) = \frac{1}{M} \int v_{out}(t) dt \tag{3.7}$$

Equation (3.7) is the expression for the current in a conductor in relation to the output voltage, measured by a RC.

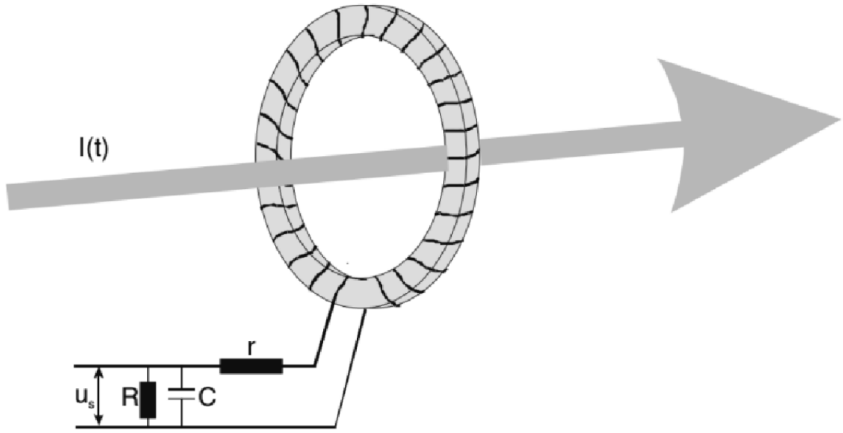

Figure 3.2: A rogowski coil with an R-C integrator [23].

The Rogowski coil has an output voltage which is proportional to the change of current, as seen in equation (3.7). Because of this, the output signal must be integrated in on order to obtain the measured current. Different ways of implementing this integration exists. The simplest integrator is an R-C integrator, shown in Figure 3.2. This integrator is a series connected resistance, and a shunt capacitor. With other words, a low pass filter. This integrator works well for the system frequency and up to over 10 kHz [62]. Active analog integrators based on Operational amplifier (OpAmp) have also been proposed [16], [23], [62]. These have the benefit of increasing the bandwidth of the integrator, but for protection applications, this is not a major consideration.

When the output voltage is integrated, the signal is shifted 90 degrees so that it is in phase with the measured current. However, delays in the integration method could add a phase shift to the signal. This causes problems when using these signals for protection applications as the compared signals will be at different amplitudes compared to their peaks at a given time. The error increases with increasing phase shift. However in [62] a small to zero phase shift was introduced by such a integrator at protection application frequencies. This effect is shown in Figure 3.3.

Digital integrators are simply microcontrollers or sophisticated machines with an algorithm which used DSP techniques to get an accurate output. Major advantages of these integrators is that DC-offset and phase shift can be dealt within the integrator. Compensating techniques can also easily be included. In [63] it was found that the digital integrators have strong rejection of digitizing noise and increasing the signal resolution. These integrators uses integration methods. For example Simpsons method, the trapezoidal method or forward Euler method [64], [65], [66] [67], [68]. Digital integrators are well suited for

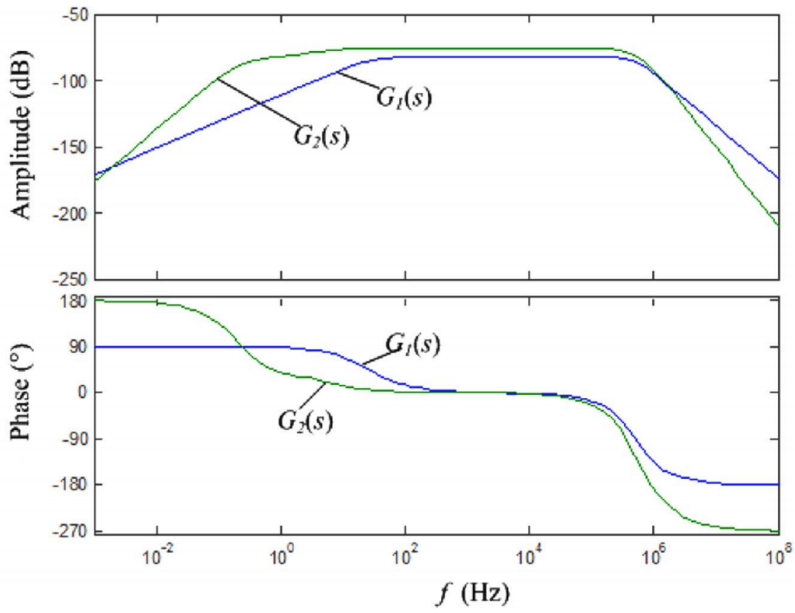

Figure 3.3: Bode diagrams of the two different integrators with the same value of R and C. $G_1(s)$ is the Measuring system (MS) based on RC with an RC integrator. $G_2(s)$ is the Measuring system based on an RC with an active integrator [62].

digital substations, as the signals should be digitized at some point anyways for use in the process bus.

3.2 Rogowski Coil Dependence on Influence Quantities

The measurement accuracy of the RC is dependant on its position in relation to the conductor and external factors. These external factors can be frequency, nearby electrical fields and temperature. In protection applications inaccurate measurements can trigger unwanted trip signals, or fail to trip during faults. Hence it is important to access how these factors affect the RC measuring accuracy, so that they can be mitigated or compensated for.

Several experiments have been conducted to affection of these factors. In [69] the position of the conductor is investigated in order to see how the eccentric positioning of the RC affects the accuracy. The authors conclude that it does affect it, but that it poses less of a challenge in protection applications as the accuracy dipped 0.01% at approximately 1.5mm offset from center. It was also found that the discontinuity of the coil has an ef-

fect on the accuracy. Denoted δ, the discontinuity is caused by the difference in the first and last turn as shown in figure 3.4. Tests performed by the same authors in [70] showed that a discontinuity of 15% introduced a significant error up to 0.5%, however, it is not expected that δ is this high in real applications. In [22] it was found that a window type RC is a lot more resistant towards eccentric positioning of the coil compared to split core type RCs. How the RC is angled compared to the conductor might also cause variations

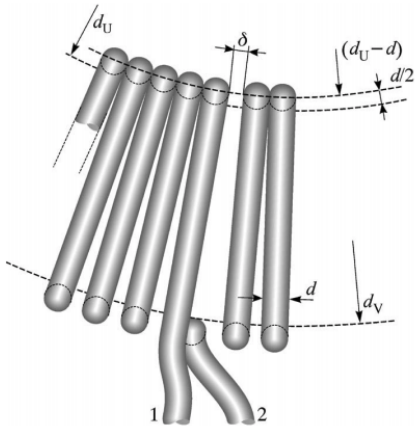

Figure 3.4: The discontinuity angle, β, to describe the angle difference between the first and last turn in the RC[69].

in the measurements. Three types of RCs is tested in the configuration seen in figure 3.5. Ratio errors of these tests are about 1% for a small split core RC and less than 0.5% for a window type RC compared to the centered reference position. It is highly unlikely that the angle of the conductor is this high in real applications, if some consideration is done when installing the RC. The tests shows that if a RC is installed in a tight location, it is better to install a properly fitting RC which does not need to be angled compared to the conductor.

Temperature variations are investigated in [71]. According to the authors, choosing a correct value load resistance of the RC is beneficial, as it acts as a voltage divider with the copper of the windings. As the temperature increases, thermal expansion occurs in the coil which in turn decreases the resistance. Furthermore as the temperature in the coil increases, more electrons and phonons collide, increasing the resistance. Hence the change in coil resistance and the thermal expansion of the coil can cancel themselves out if the load resistance is chosen appropriately. The temperature dependence is seen in figure 3.6. The accuracy is changed only in Parts per million (ppm) in relation to the temperature which indicates that variations in temperature within reasonable ranges should not affect the accuracy in protection applications in a significant way.

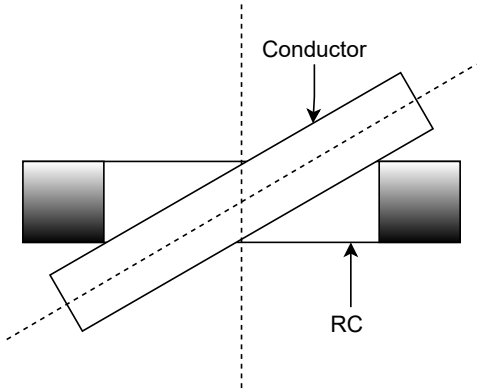

Figure 3.5: Position of angled conductor in laboratory tests [22].

Nearby conductors generate electric fields, which can disturb the RC measurements in locations with lots of equipment. Substations is an example of such a location. Ideally, the RC should only react to currents in the conductor passing through it, but this is not necessarily the case. Two design choices exists to protect against external electric fields. One possibility is to wound to opposite directed coils together, such that external fields are cancelled by the opposing coils. Another, easier method is to return a single wire through the RC as shown in figure 3.1a. It is argued that the internal return wire loop does the same job, but with an easier implementation [15]. In tests conducted by [71] less than 0.005% error is recorded for distances higher than 0.4 m from the RC was introduced from external conductors for a split core type RC.

Tests have also been done on RC in order to evaluate how multiple influencing quantities affect the accuracy of the measurements. [22] studies the combination of conductor position, temperature and frequency variations combined. In these tests three types of RCs were tested; one window type RC, and two split core type RCs. A window type RC cannot be opened, which means the conductor must be passed through it. The split core type can be opened, and can hence easily be placed around a conductor. This however, has a disadvantage because it increases δ and usually means it is less circular. [22] finds that frequency deviations does not affect the RC measurements, but that a combination with different positions and high and low temperatures has a great impact on the measurements. For use in protection applications, the RC measurements needs to be dependable under all conditions. If an inaccuracy is included in a RC in a differential protection scheme, it may cause inadvertent triggering or failure to do so under faults. Both cases would result in a malfunctioning differential protection scheme. Especially is the failure to trigger a fault under extreme contingencies a critical point, as the spread of a contingency can cause major damage to infrastructure, the environment or life. Hence, a RC used in protection

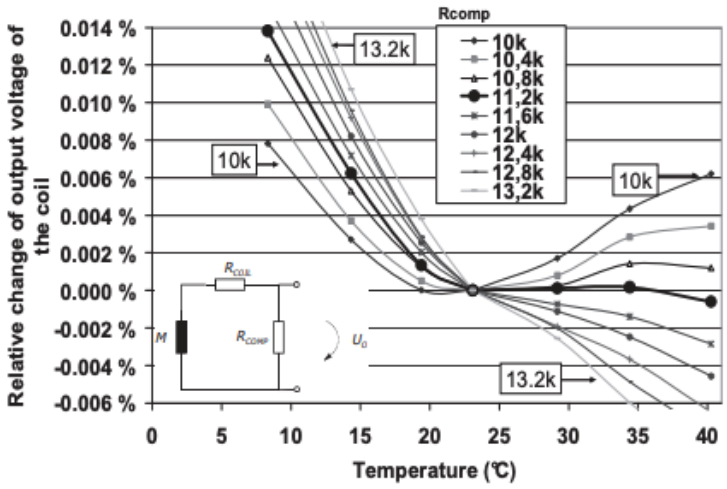

Figure 3.6: Temperature dependence in RC with different load resistances [71].

applications must work under all scenarios. It is important to gain an understanding on how influencing factors affect the measurements, and to introduce methods to compensate for the influencing factors.

To quantify the measurement accuracy of the RC, a standard is defined. In IEC 61869-9 Digital interface for instrument transformers. It defines requirements for digital communication of instrument transformers with digital output [72]. Within IEC 61869-9 a definition for the calculation of measurement accuracy is included. This is called composite error and is used for all instrument transformers including conventional CTs. The composite error can be calculated as:

$$\epsilon_c(s) = \sqrt{\frac{\sum_{n=0}^{N-1}\left[(i_{X(s-n)} - i_{R(s-n)})^2\right]}{\sum_{n=0}^{N-1}\left[(i_{R(s-n)})^2\right]}} \cdot 100\% \tag{3.8}$$

Here $\epsilon_c(s)$ is the composite error at a time instant s. $i_{X(s)}$ is the measurement value of the instrument transformer at s. $i_{R(s)}$ is the value of the reference instrument transformer at s. N is the nominal sample rate in samples per second divided by the fundamental frequency in hertz.

To investigate the overall composite error of the RC, equation (3.8) can be modified

slightly to exclude s, and hence becomes:

$$\epsilon_c = \sqrt{\frac{\sum_{n=0}^{N-1}\left[(i_{X(n)} - i_{R(n)})^2\right]}{\sum_{n=0}^{N-1}\left[(i_{R(n)})^2\right]}} \cdot 100\% \tag{3.9}$$

Using this formula, it is possible to compare the overall error of a RC compared to a reference CT.

3.3 Laboratory Setup

The RC accuracy tests are conducted in an ad hoc laboratory test rig designed with help from Mr. Katoulaei and the service lab at Department of Electrical Engineering. The test rig is seen in figure 3.8a. Two aluminium hollow conductors are fastened to the test bench

Figure 3.7: The Fluke i2000 flex used in laboratory testing [73].

through adjustable stands. These are placed on horizontal plates where the fasteners can slide to adjust the position of the conductors. Rulers placed to the side of the horizontal plate allows for millimetre adjustments of the positions and arrow indicators on the conductor stand clearly shows its placement relative to the ruler. The horizontal adjustment is shown in figure A.2. A RC in test is fastened to a frame which is held up by the test

rig. The RC is seen in figure 3.8c. It is connected through a cylindrical arm attached to a cylindrical stand which allows for vertical adjustments as seen in figure A.6. The use of cylindrical components allows for adjustments in how the RC is angled compared to the conductors. The frame height can also be adjusted by sliding the arm relative to the stand. Protractors and arrow indicators are used to assist in adjusting the angles as seen in figure A.7 and figure A.8. The RC used is a window type Fluke i2000 Flex as seen in figure 3.7.

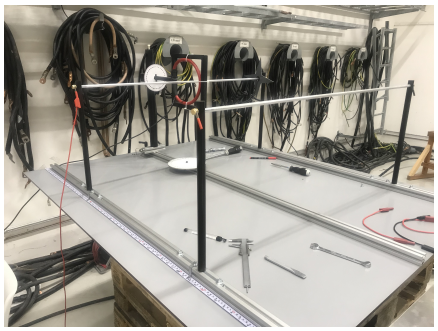

(a) The test rig.

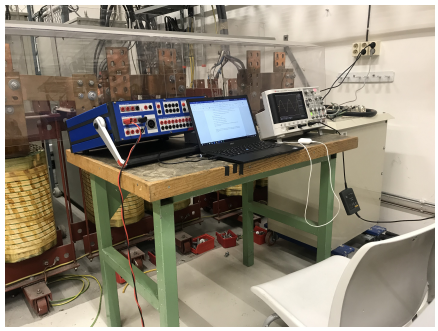

(b) The test devices. Left: Omicron, right: oscilloscope

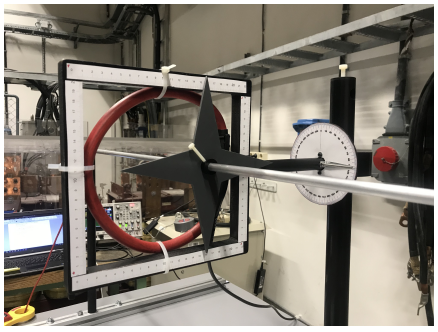

(c) The RC frame. Position indicators glued to the frame, star contraption to verify adjustments which aligns with position indicators.

(d) Omicron CRC 356.

Figure 3.8: Photos from the laboratory setup and the equipment used.

It has a current rating of 200 A or 2000 A and an integrator. It has a large window suitable for high current conductors. The flexible build means it can be installed easily in a range of locations. However, because of this it does not hold a rounded shape well. It is locked by a clip, the black part of RC in figure 3.7 and figure A.5. Fluke does not advertise the number of turns or the discontinuity, δ. The accuracy is rated at $\pm 1\%$ [74].

A Pearson Electronics Inc. current monitor referred simply as CT, shown in figure A.9, is used as a reference to compare the RC measurements and compute its error. The CT has an error of $+1\%$ according to the producer [75]. Both transducers are connected to

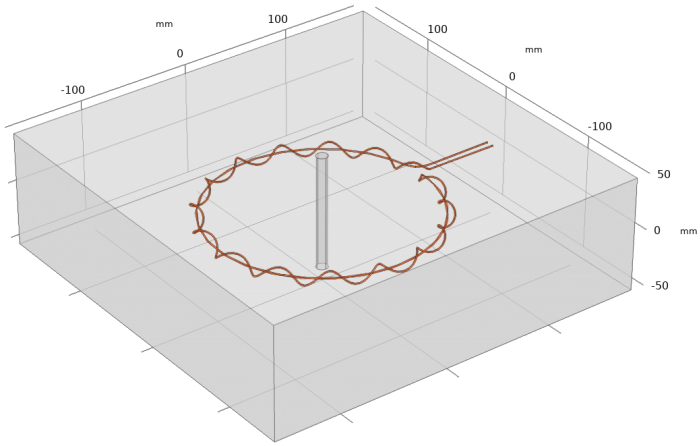

Figure 3.9: The RC model in orange with the air domain around the coil and the conductor in the middle of the figure. The terminals of the RC is seen on the right.

a InfiniiVision 2000 X-Series oscilloscope by means of coaxial cables. The test current is generated by an Omicron CRC 356 relay test set seen in figure 3.8d. The Omicron is able to output currents at different output levels and frequency 32 A banana plug cables are connected via the Omicron to the test rig conductors, figure A.4, hence limiting the output current to 32 A. A computer with the Omicron Test Universe software is used to configure the output of the Omicron. The Omicron, computer and oscilloscope is seen in figure 3.8b. A schematic of the laboratory setup is shown in figure A.1 displaying the connections without the test rig shown.

3.4 Finite Element Method Modeling Setup

A RC FEM model is built in COMSOL Multiphysics. It consists of a cylindrical conductor, enclosed by the coil. The coil is built from wound copper cables with a radius of $r_{wire} = 1.5$ mm. The coil has a major radius $R = 97.5$ mm and a minor radius $a = 5.6$ mm. The minor radius is the radius of each winding. The radius of the conductor is 5 mm. For the coil, the return wire concept is utilized to protect against external fields.

Parametric curves are drawn in the model, and represented by three expressions in three dimensions

$$
\begin{aligned}
x &= (R + a \cdot \cos(d\pi\theta)) \cdot \cos(\theta) \\
y &= (R + a \cdot \cos(d\pi\theta)) \cdot \sin(\theta) \\
z &= a \cdot \sin(d\pi\theta)
\end{aligned} \tag{3.10}
$$

Here, θ is the angle of the parametric curve, stretching from 0 to $2pi - \delta$. The resulting curve has a helix shape which is distributed in the XY-plane as a circle with a given radius, a, offset from origo with R. The radius of the RC, R, is 97.5 mm. The radius of each winding, a, is 5.6 mm. This curve does not have a thickness. Therefore, a circle with the radius, r_{wire}, is swept along the curve which results in a 3D coil using a sweep function. The parameter d determines the density of the windings where a higher number increases the number of turns and the simulation time. It is set to a quite low value of 5, which results in 16 turns. If this value is increased, the sweep function is more likely to return invalid geometries. The return wire is created using the same method, but is not circled up to a helix like the windings. Hence, the z-component is zero. With no variation in the x- and y-dimension as well the expressions for the return wire become

$$x = R \cdot cos(t) \tag{3.11}$$

$$y = R \cdot sin(t) \tag{3.12}$$

$$z = 0 \tag{3.13}$$

The coil structure has a homogeneous distribution except for the discontinuity and the connection to the return wire. The discontinuity of the coil is set to 1° which is set arbitrary to match a possible discontinuity of a real RC. The terminals of the RC can be in an open circuit configuration or connected to an output resistance.

Insulation is created around the windings with a thickness of 1 mm. The insulation is spaced so that there is a gap between the windings and the insulation. This geometry however, increases the mesh complexity as fine mesh elements has to be created inside the windings. This further requires fine mesh elements in the gap between the windings and the insulation, and additionally, in the insulation. Due to this, the simulations are run without the insulation as it should not affect the results because insulation material has a low permeability. The rest of the volume inside the RC is air. This is done by adding a box around the RC which is defined to contain air.

The model uses the *magnetic fields* interface with the coil module to simulate the mag-

Table 3.1: Physics nodes used in the *magnetic fields* interface in the model.

Node	Applied for
Ampère's law	Air & insulation
Magnetic insulation	Exterior boundaries
Initial values	All domains
Coil 1	Conductor
Coil 2	RC

netic fields and the current excitation. Table 3.1 shows a summary of the physics nodes used in the model under the magnetic fields interface. The Ampère's law node makes it possible to look at induced current through the coil. The magnetic insulation creates a boundary of no magnetic field propagation on the exterior boundaries in the model. The initial values node ads a initial magnetic field to the model, which in this case is set to zero everywhere. The coil nodes is used to study the mutual inductance between the conductor and the RC. With Ampère's law it allows for the modeling of the induced voltage in the RC. The conductor is set to have a current of

$$I = 100\sin(2\pi ft)[\text{A}] \tag{3.14}$$

An output resistance can be connected to the RC by adding an "electrical circuit" physics to the simulation. This is coupled with the "magnetic fields" physics, which increases the complexity of the simulation. By coupling these physics, the influence on the output resistance can be tested.

In order to simulate the model a mesh is required. Due to the thin wires, a fine mesh

Table 3.2: Mesh statistics for the model when the conductor is in its centered position.

Property	Value
Mesh vertices	19383
Tetrahedra	112853
Triangles	7154
Edge elements	2992
Vertex elements	40
Minimum element quality	0.1577
Average element quality	0.6258

is needed in this area. The rest of the model can be meshed with free rules with a coarser mesh setting. Table 3.2 shows a summary of the mesh statistics in the model. Tetrahedral elements are 3D elements which are highly represented in the model. The triangle ele-

ments are used in the windings and the conductor to to their swept geometries. Generally COMSOL recommends a minimum element quality which is above 0.1 for most physics.

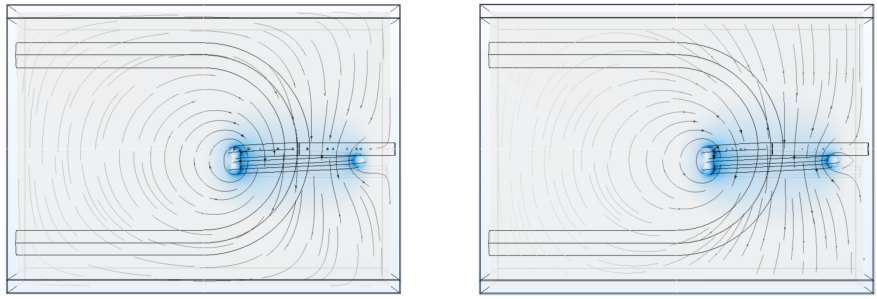

(a) Without infinite element domains **(b)** With infinite element domains

Figure 3.10: Magnetic field in a simple coil model showcasing the effect of infinite element domains. Infinite element domains are not added to the left and right side due to terminal connections of the conductor and the coil. Current is excited in the coil on the right side, and induces a voltage in the U shaped conductor. The blue color shows the magnetic field strength, and the curves shows the direction of the magnetic field.

It is possible to simulate a big air domain around the model by using a infinite element domain. The infinite element domain stretches the outer region of the air domain with mathematical functions. This is beneficial as it means the physical laws are not limited by the region of the model. Hence, magnetic fields are allowed to spread as they naturally would. Figure 3.10 shows a comparison between the magnetic field in a arbitrary coil model comparing the effect with and without infinite element domains. The use of infinite element domains are expected to yield more accurate solutions because of this.

Chapter 4

Laboratory Testing & Finite Element Method Simulations

Tests conducted in the laboratory setup described in the previous chapter and simulations using the FEM model is included in this chapter. The laboratory tests are conducted to assess the accuracy of the RC and to act as verification for the FEM model. Conductor position adjustments are conducted for both the laboratory tests and the simulations.

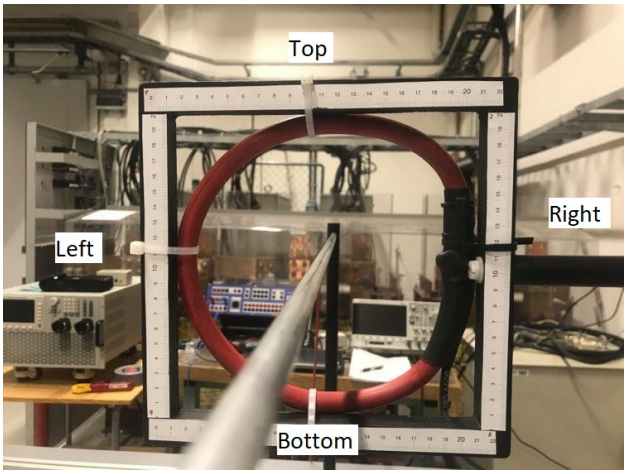

Figure 4.1: The RC in the test rig frame with side references indicated with text. The RC opening is the black part on the right side. The conductor is seen as the grey bar in the middle.

4.1 Laboratory Tests

The laboratory tests are split into horizontal adjustments, vertical adjustments and diagonal adjustments of the current carrying conductor position. The conductor is adjusted in

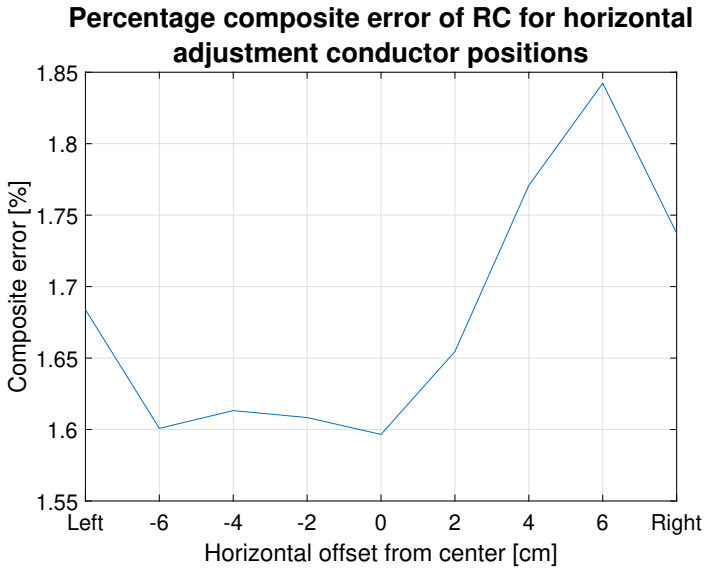

Figure 4.2: Laboratory test percentage composite error of RC for horizontal adjustments of conductor position.

steps of two centimeters. From the step of six centimeters for the horizontal and vertical adjustments, the step of eight centimeters is skipped. The conductor is instead adjusted slightly more until the conductor adjoins with the RC insulation surface. These positions

Table 4.1: Oscilloscope measured RC and CT RMS values from vertical adjustments.

Position	RC RMS [A]	CT RMS [A]
Top	29.79	29.93
6	29.80	29.94
4	29.81	29.94
2	29.79	29.94
0	29.84	29.95
-2	29.84	29.94
-4	29.89	29.95
-6	29.94	29.95
Bottom	30.07	29.95

Table 4.2: Oscilloscope measured RC and CT RMS values from horizontal adjustments.

Position	RC RMS [A]	CT RMS [A]
Left	29.78	29.94
−6	29.85	29.93
−4	29.86	29.94
−2	29.85	29.93
0	29.83	29.95
2	29.77	29.93
4	29.71	29.95
6	29.66	29.94
Right	29.74	29.95

is denoted *end* simply because measuring the offset from center is difficult with the equipment available in the lab. Furthermore, the sides are denoted such that the right side is the side where the opening on the RC is. This is done for readability purposes.

Horizontal adjustments are tested with 2 cm increments in both directions from the central position. The measured RMS current from the oscilloscope is shown in table 4.2. Figure

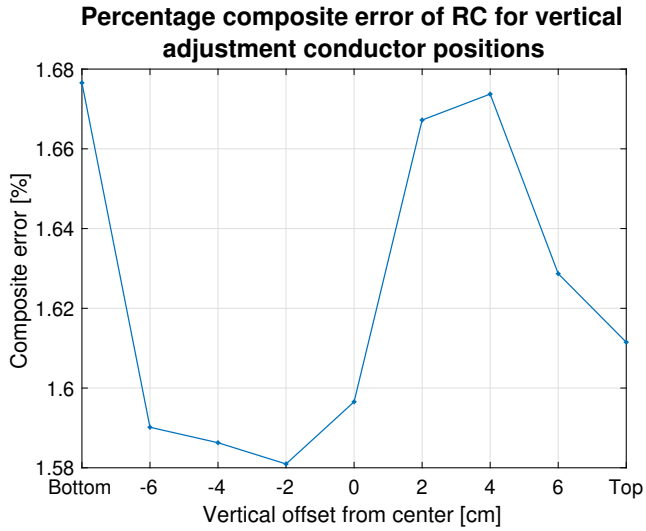

Figure 4.3: Laboratory test percentage composite error of RC for vertical adjustment of conductor position.

4.1 summarizes how the sides of the RC is denoted in the text. For each position five measurements are done in roughly ten seconds intervals. Composite error is calculated from the average composite error of each signal using equation (3.9).

4.1.1 Horizontal Adjustments of Conductor Position

The horizontal adjustments are somewhat constant towards the left side, ie. the one opposite to the RC opening on the right side. Towards the opening it picks up lower values. This is reasonable due to the discontinuity. Figure 4.2 shows the percentage composite error for the horizontal adjustments. The error actually decreases from the centered posi-

Table 4.3: Oscilloscope measured RC and CT RMS values from diagonal adjustments. H. pos - horizontal position and V. pos - vertical position.

H. pos [cm]	V. pos [cm]	RC RMS [A]	CT RMS [A]
2	2	29.80	29.96
4	4	29.82	29.94
6	6	29.94	29.95
Top	Right	29.99	29.95
2	−2	29.83	29.95
4	−4	29.80	29.95
Top	Left	29.82	29.94
−2	−2	29.81	29.95
−4	−4	29.75	29.96
−6	−6	29.64	29.95
Bottom	Left	29.62	29.96
−2	2	29.90	29.95
−4	4	30.00	29.96
Bottom	Right	30.03	29.95

tion as the conductor is moved towards the left end. This can be an effect of the RC not being perfectly round, which offsets the real center. The error in the centered position is 1.6%, which is very high. It varies with 0.25 percentage points. Both directions show clear trends, but the endpoints are differing from these. The endpoints are also quite equal, compared to the six centimeter adjustments in both directions.

4.1.2 Vertical Adjustments of Conductor Position

The same tests are conducted in vertical increments and the results are shown in table 4.1.

The vertical adjustments also differ from which direction the adjustments are done. Upwards the values decreases somewhat, while downwards the values increases. The accuracy varies with 0.1 percentage points. The difference between the upward and downward adjustments can be due to the discontinuity which is not symmetrical around the horizontal center. Hence the effect from the discontinuity is likely different.

4.1.3 Diagonal Adjustments of conductor Position

Some diagonal tests with equal vertical and horizontal increments are supplemented.

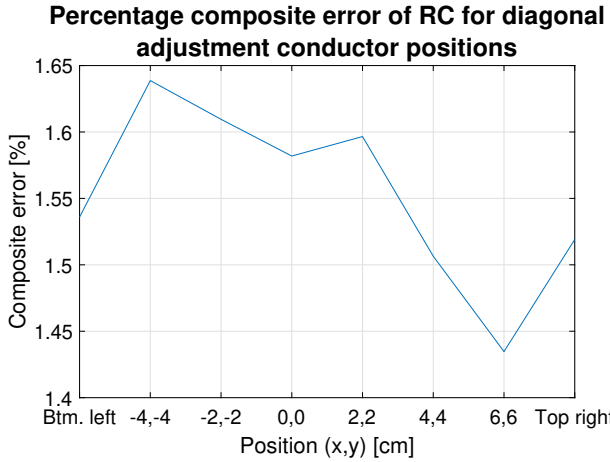

Figure 4.4: Laboratory test percentage composite error for diagonal adjustments from bottom left to top right of RC window.

Due to the structure of the RC all positions are not available as the locking mechanism adds some stiffness to the structure, which in turn makes the two sides closest to the opening less round. Hence, it is not possible to make this particular RC perfectly round. Additionally,

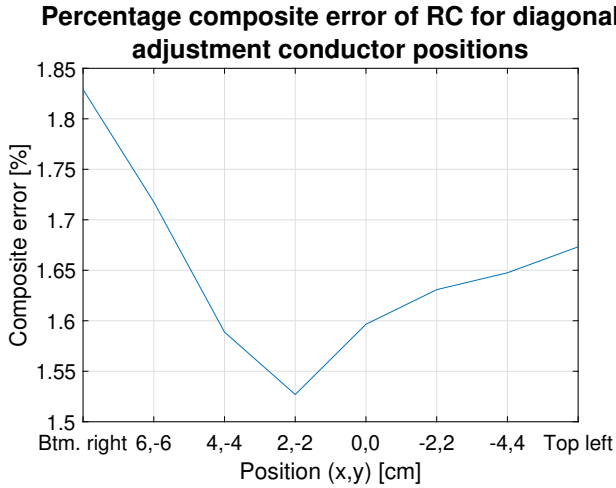

Figure 4.5: Laboratory test percentage composite error for diagonal adjustments from bottom right to top left of RC window.

this means the diagonal adjustments have four measuring steps in the directions towards the RC opening side, whereas the other two have three adjustment steps. The figures use the notation ”top left” and ”bottom right” etc. to refer to adjustments which adjusts the conductor towards the top and left side and bottom and right side of figure 4.1 respectively. These notations are used because the exact conductor offset has not been possible to measure. The measured RMS values of each diagonal position is presented in table 4.3. The

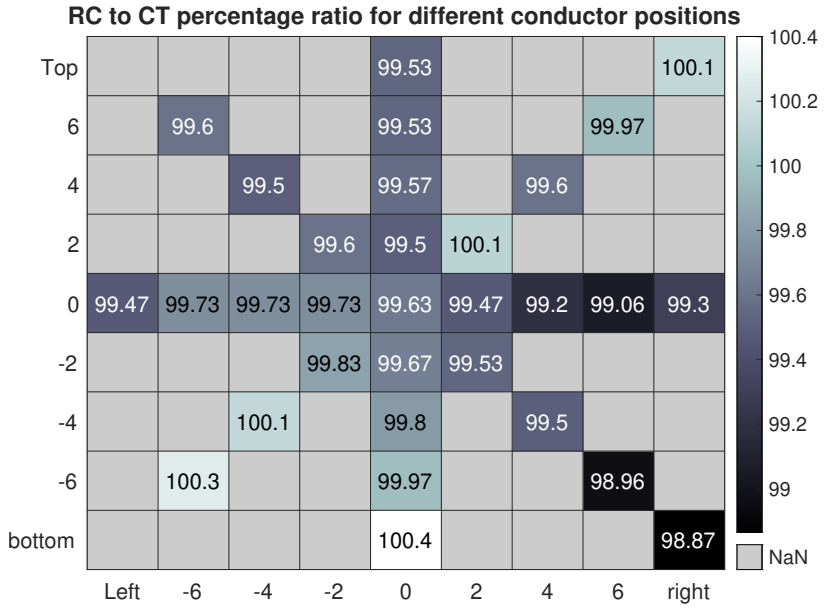

Figure 4.6: Heatmap showing the percentage ratio between the measured RMS of the RC and the CT for different conductor positions. A high value above 100 indicates that the RMS for the current conductor position is higher than the CT RMS current.

composite error for the diagonal adjustments are shown in figure 4.4 and figure 4.5. The adjustments from bottom left to top right have opposite effects but are generally quite low, peaking at less than 1.65%. The diagonal adjustments from bottom right to top left show quite a clear trend, but have significantly higher errors compared to the other diagonal adjustment.

A heatmap showing the ratio between the RC output and the reference CT is shown in figure 4.6. The heatmap explains why some positions have lower composite error. When the ratio increases which is seen for the diagonal adjustments from bottom left to top right, the errors decreases. This is due to the RC output being significantly lower than the CT in general. The heatmap shows a strong variance in the output in the RC window. Towards

4.1.4 Influence from External Conductors

The terminals of the Omicron is connected to the external conductor, and the conductor is moved such that it is in contact with the RC insulation. The RC readings are shown in figure 4.7. No current is going through the main conductor. The oscilloscope is not able to pick up any differences in the RC measurements when the external is dead and when 30 A is going through it. When no current is active, the oscilloscope reads up to 1 A which is a significant level. This is due to the oscilloscope, because this value is independently of whether the RC is on or not. There likely exists some measure or setting to remove this error but this is not done during this work. The amount of noise when the RC is not

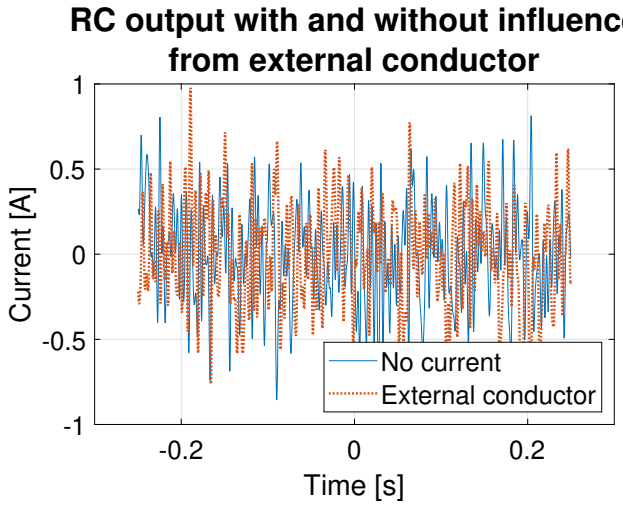

Figure 4.7: Current output from RC with no current in any conductors, and with 30 A in external conductor adjoined with RC insulation.

outputting anything is very high and makes it difficult to analyse the effect of the external conductor, but these short tests indicates that the return wire is successfully able to cancel any stray fields outside the RC window.

4.2 Finite Element Method Modeling Simulations

The RC model simulations are performed using parametric sweeps in COMSOL. These sweeps simulates different parameters in the same run. The simulations are organized such that a range of conductor positions are tested for a homogeneous distributed RC for a 100 A, 50 Hz conductor current. Conductor positions are tested in 20 mm increments

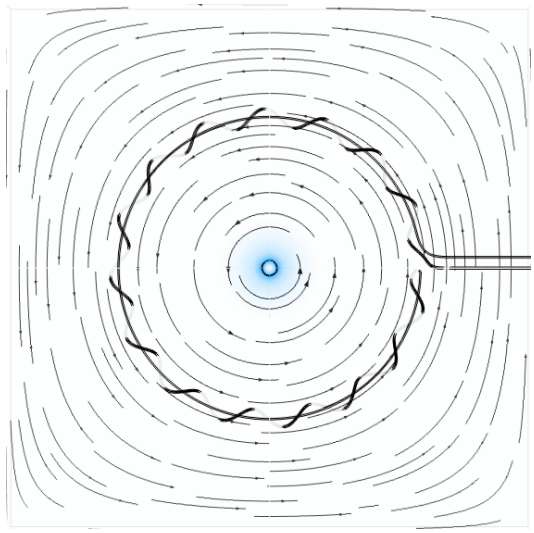

Figure 4.8: Magnetic field distribution in COMSOL RC model. Model shown from XY-plane. Conductor in centered position with 1° discontinuity.

in the horizontal, vertical and diagonal directions. The last steps are simulated such that it adjoins with the insulation which is not used in the simulations. The last step for horizontal and vertical adjustments are hence 83 mm, which leaves a gap of slightly more than 1 mm to the windings. Simulations are done with and without an IED. With an IED the linear solver requires significantly more iterations to solve, which increases the solution time. Tests on a simple coil model showed that the linear solver required three iterations per time step on average without the IED, while it required 198 iterations per time step on average with the IED. For the RC model, this means the simulation time is increased tremendously. Because the current carrying conductor is placed in the middle of the air domain, and since the RC is very big, a air domain without infinite element domains does not limit the spread of the magnetic field. Infinite element domains are therefore not used in these simulations. Instead, a larger air domain is used which allows for more space for the propagation of the magnetic field. Figure 4.8 shows the magnetic field in the air domain from the XY-plane. In the figure, the effect on the limited air domain is visible, but does not seem influence the RC window greatly.

Table 4.4: Materials used in RC model.

Material	Used on	Rel. permeability	Rel. permittivity	El. conductivity [S/m]
Copper	Windings, conductor	1	1	1000
Air	RC interior, ext. space	1	1	0.0001

Before simulating the physics in the model, a coil geometry analysis is conducted. This is done because the coil physics node is used. In both the conductor and the RC an input and output boundary is chosen. The coil geometry analysis calculates the path of the wire within the domains from the input to the output. Figure B.1 presents the calculated directions for both the conductor and the RC. The arrowheads in red follows the windings which indicates that the coil geometry analysis is successfully calculating a clear path along the swept windings. When the coil geometry analysis is done, a time dependant simulation is calculated. A linear solver calculates the time steps using adaptive time stepping for a whole period from 0 to 20 ms.

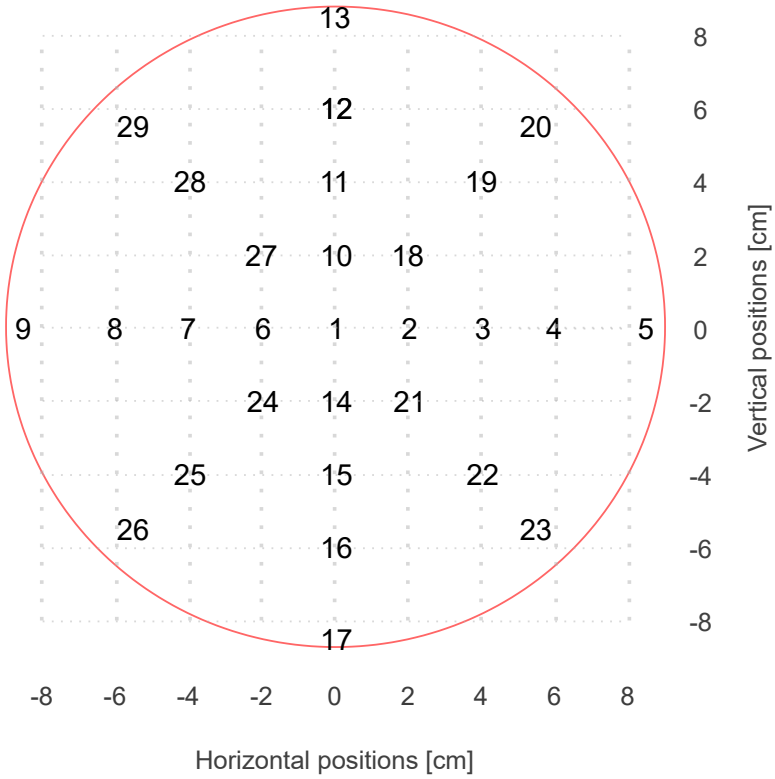

Figure 4.9: Test numbers of conductor positions in RC window in the simulation model. The red circle represents the RC

Some parametric sweeps are conducted on different material conductivity values. Instead of using the standard values, these values makes the simulations easier to solve if they are changed closer to 1. It is found that for copper the value does not influence the result much, thus it is set to 1000 S/m. For air the results are influenced for values less than $1e{-}4$ S/m, but not improved for values above this. For values less than $1e{-}5$ S/m, the simulation time

is greatly increased as the simulation struggles to make long time steps. Hence a value of $1e{-}4$ S/m is used for air. The materials used in the model is summarized in table 4.4.

4.2.1 Conductor Positions for 16 Turns Configuration

A parametric sweep is conducted over several conductor positions in the model. Figure 4.9 shows all the tested positions in the RC window. They are also summarized in The positions are summarized in table B.1. The composite error for all positions are shown in figure 4.10 for the homogeneous distributed RC with $\delta = 1°$.

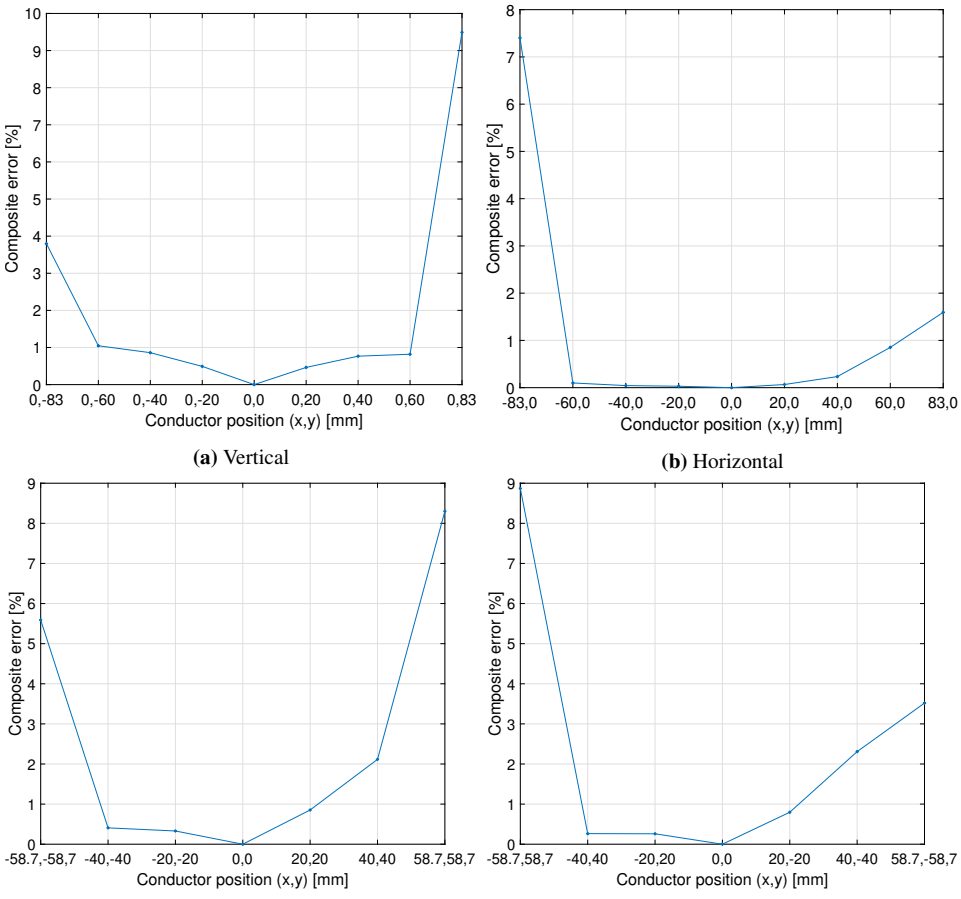

(a) Vertical

(b) Horizontal

(c) Diagonal for equal signs

(d) Diagonal for opposite signs

Figure 4.10: Composite error for all 29 conductor positions in subfigures showing a sweep from one side to the other with the centered position in all figures. Homogeneous winding distributed with $1°$ discontinuity.

The results tend to show some general trends. In the vertical adjustments, the error is quite equal up to 60 mm. This is likely due to the position of the discontinuity. Hence, the vertical positions have a more symmetrical result. The composite errors from the horizontal adjustments are not intuitive, as the error greatly picks up in the end position on the opposite side of the discontinuity. The error for positions equal and less than 60 mm is however higher when adjusted towards the discontinuity. Figure 4.10b, figure 4.10c and figure 4.10d all have higher composite errors towards higher x-coordinates, which indicates that the error is higher when the conductor is positioned towards the discontinuity. The error picks up greatly when the conductor position approaches the end. This effect is not always the same in opposite as is clearly seen in all cases where the composite error varies between 2.7 to 5.8 percentage points for figure 4.10c and figure 4.10b respectively. Compared to the laboratory tests, the simulated errors differs more from the centered posi-

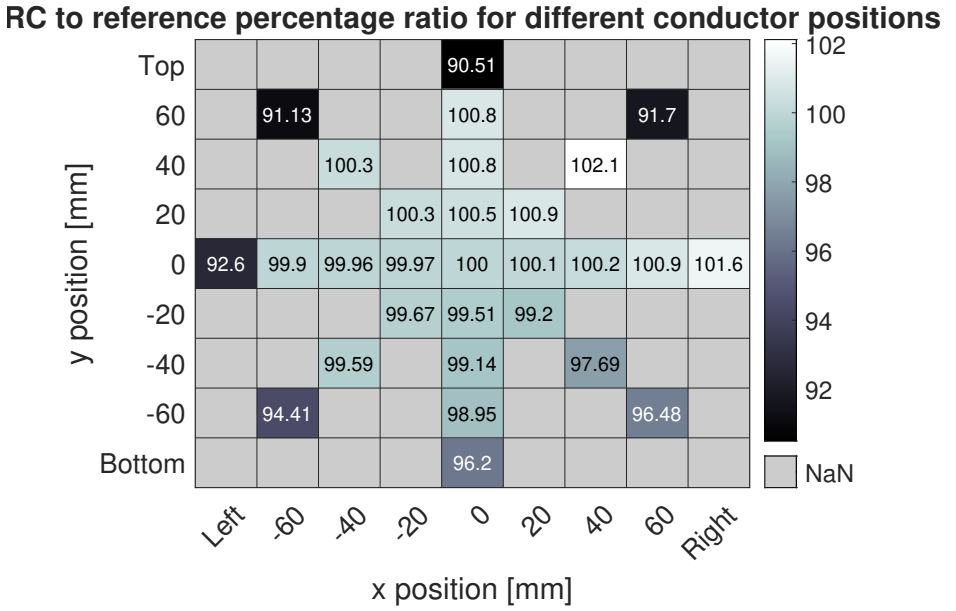

Figure 4.11: Ratio between the measured RMS voltage of a position compared to the centered position in per cent.

tion. Additionally the error in the end positions did not always increase in the lab. In some of the lab tests the error actually decreases for the end position. A heatmap for the ratios between the reference voltage and the voltage outputs for the different conductor positions is found in figure 4.11. As expected, the the ratio is low in the end points. However for positive x positions the values are actually increasing. This in contrast to the laboratory tests. In figure 4.6 the ratio is low for increasing x-values. Another surprising result is that

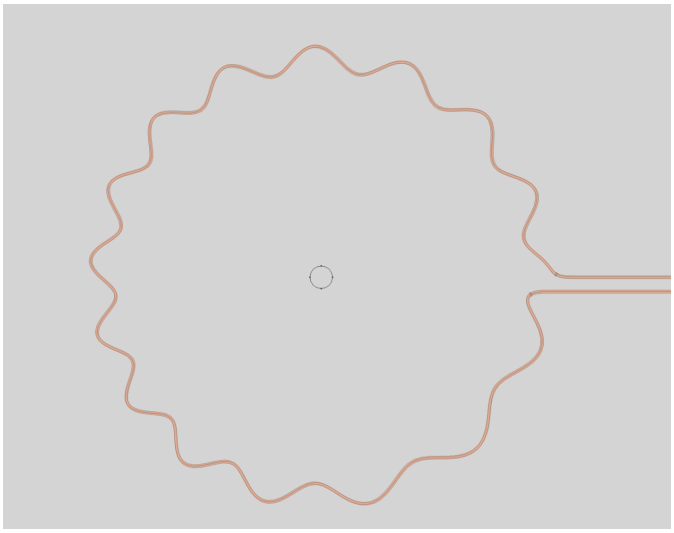

Figure 4.12: 16 turn inhomogeneous winding distribution seen from xy-plane for RC with $\delta = 4°$. No return wire.

the ratio is above 100% for all positions where $y < 0$ except for the end points. As the windings are homogeneously distributed, this effect must be attributed the discontinuity.

4.2.2 Conductor Positions with Inhomogeneous Winding Distribution

The lab results differs significantly from the simulation results, and this can be attributed to randomness in the winding distribution in the real RC. To investigate this effect, a RC with an inhomogeneous winding distribution is created. This is done by inserting a sine function for the winding parameter, d, in equation (3.11). Because of the added complexity this gives for the sweep function, the return winding is removed. Because the return winding is removed, a higher δ is required to make a gap between the terminals. This is because small regions are difficult to mesh. The winding parameter is chosen such that the value of d becomes

$$d = 5.2 + 0.2\sin(1.4 \cdot \theta + \frac{\pi}{1.5}) \tag{4.1}$$

The constant value, 5.2, determines the base frequency, and the sine function creates a variance in the base frequency which varies with the angle, θ, of the circular geometry. This results in a winding which is wound tighter from the positive terminal, is gradually

wound looser, then tighter, and lastly loose again. The inhomogeneous geometry is seen in figure 4.12.

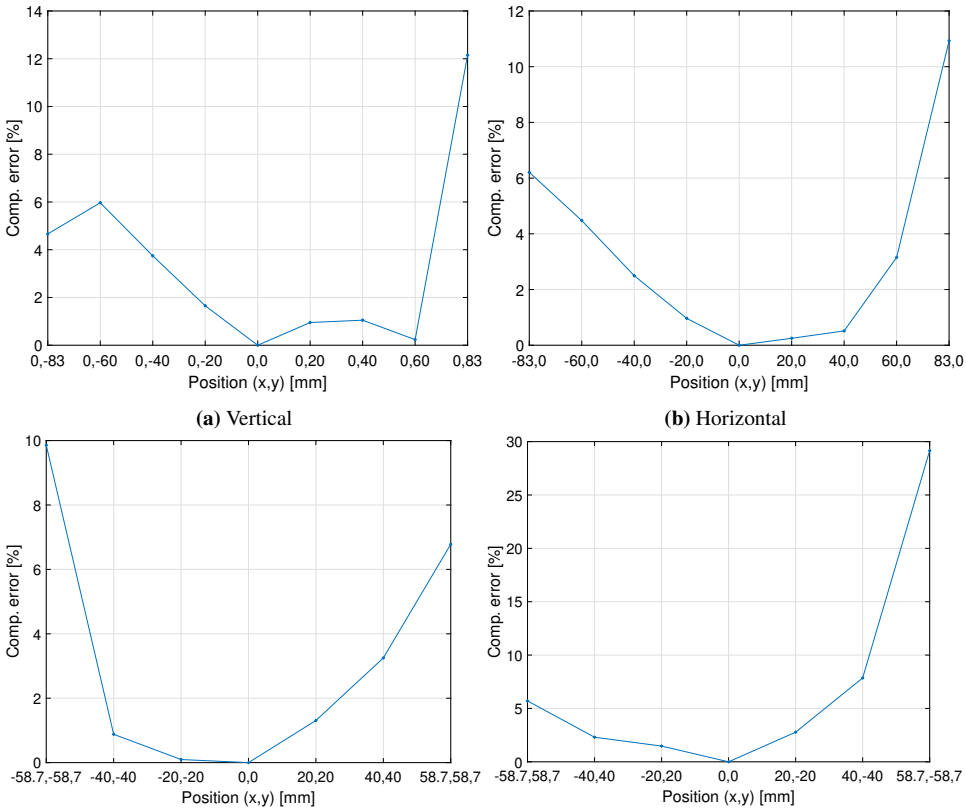

(a) Vertical

(b) Horizontal

(c) Diagonal for equal signs

(d) Diagonal for opposite signs

Figure 4.13: Composite error for all 29 conductor positions in subfigures showing a sweep from one side to the other with the centered position in all figures. 16 turn inhomogeneous winding distributed with $4°$ discontinuity. No return wire.

The inhomogeneous winding distribution does not make a significant change in the trends for most conductor position adjustments as seen in figure 4.13, but the vertical positions, seen in figure 4.13a have developed a similar, but opposite, effect compared to figure 4.3. Appendix B, figure B.2 shows both figures for comparison.

4.2.3 Conductor Positions for 48 Turns Configuration

The low number of windings is possible one explanation for the difference between how positional adjustments influences the error in the laboratory tests and the simulation tests.

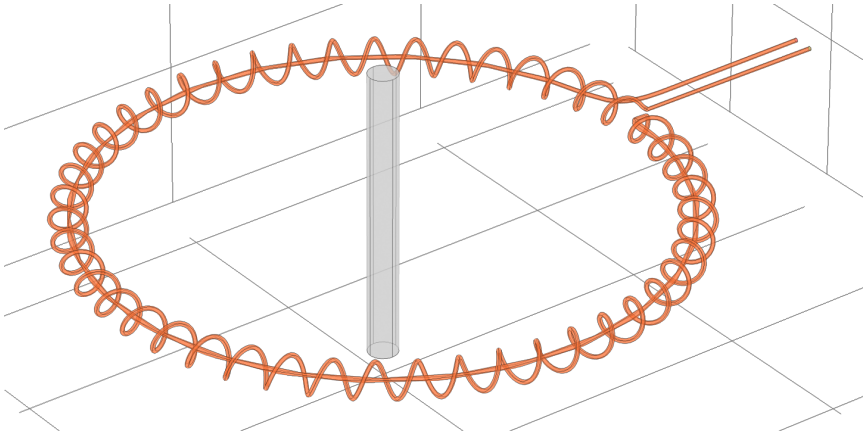

Figure 4.14: The geometry of the RC in orange with 48 turns and return wire. Grey conductor in the centered position. Discontinuity shown in the top right corner with the output terminals.

While the difference between the highest and lowest accuracy for the horizontal laboratory tests is 0.25 percentage points, the same simulation test results in 5.8 percentage points when $n = 16$ turns.

To test if the model number of windings initially is set to low, d is increased to 15. This yields three times more windings such that $n = 48$ as seen in figure 4.14. While still a relatively low number compared to what is possible in real applications, it is significantly higher than in previous simulations. Increasing the number of turns above this with the current method of building the geometry is likely to fail. With a high number of turns, the sweep function must analyze steeper curves, which increases the chance of crossing edges or other critical errors.

The positional tests are redone with the new winding density in a homogeneous distribution for the conductor positions in figure 4.9. The resulting composite error plots are shown in figure 4.15. In this case the composite error is significantly lower than in the low turns case. The values of the composite error is in the same area as in the laboratory tests. The end effect is also not occurring, except for the diagonal adjustment in figure 4.15d. Horizontal adjustments towards the discontinuity is still strong The diagonal adjustments are also heavily influences when the conductor is adjusted towards the discontinuity ie. for positive x-values.

Figure B.3, B.4, B.5, B.6 show the phase shift for the various conductor positions. A negative phase shift means the particular conductor position lags the centered position. The phase shift is significant, and generally negative, or lagging, the centered position.

Only when the conductor is placed towards the discontinuity is the phase shift positive. The difference between the vertical adjustments shows how the discontinuity placement, located with positive y-component, affects the phase shift, even when located far away from the discontinuity.

4.2.4 Effect of Discontinuity

As the discontinuity has a great impact on the composite error of the RC, a parametric sweep of some discontinuities are done. The discontinuity values and their composite error for a $y = 20$ mm conductor position compared to their centered position is shown in table 4.5. It is possible to achieve a negative discontinuity because the windings does not overlap. The ratios indicate that high values, both positive and negative, for the

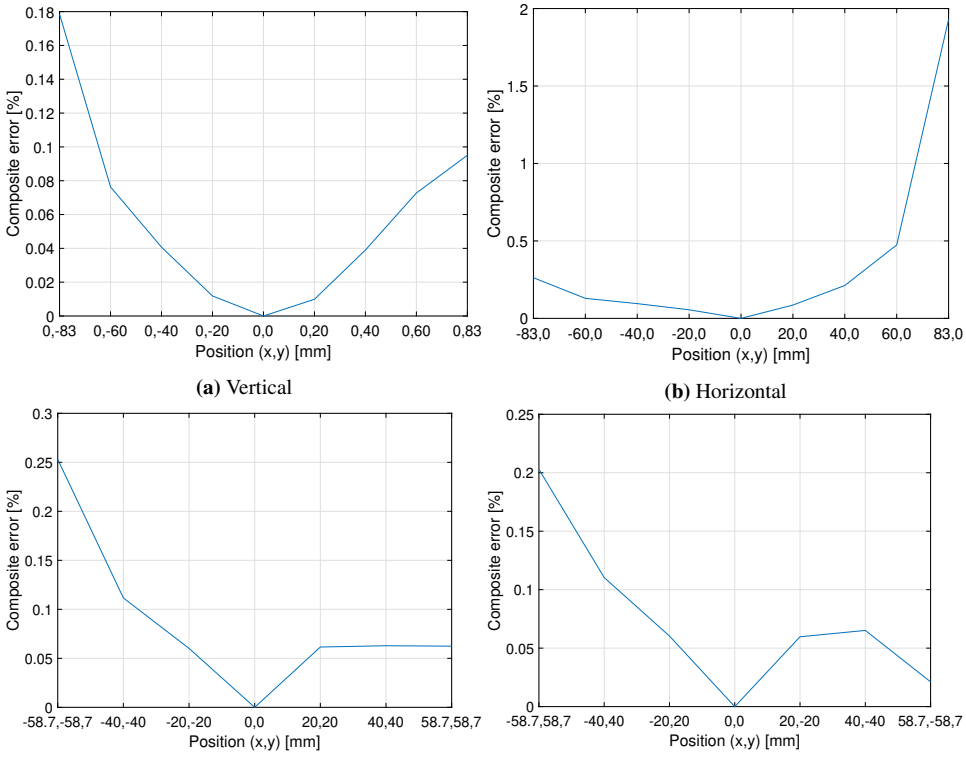

(a) Vertical

(b) Horizontal

(c) Diagonal for equal signs

(d) Diagonal for opposite signs

Figure 4.15: Composite error for all 29 conductor position adjustments for a RC with $d = 15$ resulting in 48 turns. Homogeneous winding distributed with 1° discontinuity.

discontinuity will result in high ratio differences compared to the reference used in this

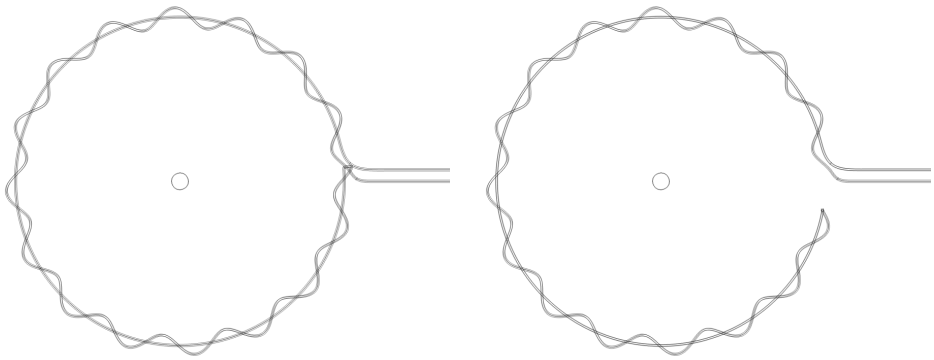

(a) $\delta = -5°$ **(b)** $\delta = 10°$

Figure 4.16: The RC geometry with different discontinuities seen from XY-plane. The discontinuity is located on the right side.

case for $\delta = 1°$. This indicates that discontinuities will give a high error. Surprisingly the composite error is the highest for the zero discontinuity case when the conductor is offset $y = 20$ mm. As the values for zero and one degree differs this significantly from each other it seems viable that the model has to be refined to get more consistent results. The model uses a sweep function to create the wires which could result in quite different geometries. The table does however seem to indicate that high and low values of δ will result in high composite errors for conductor offset. Note that this model does not give proper measurements as it does not have an integrator. Hence it is not possible to compare the results to a true reference. Therefore the ratios can not be used to conclude on which discontinuity is the most accurate, but it can be used to get an impression on how the discontinuities changes the readings.

4.2.5 Effect of Output Resistance

Simulations are performed on three output resistances when using the additional electrical circuits physics node. As the previous simulations are done in an open circuit configuration, currents have not been seen yet. These tests hence aims to verify the physics of the model by adding the complexity of the output circuit. All these tests are done in the centered position. Figure B.7 shows the current densities in the coil and in the conductor. Note that by the right hand rule, the coil is directed from the return wire via the windings. This effect is not expected, given the name *return* wire. It could be that the RC has too few turns. It is also possible that this is a limitation of the model, but as COMSOL is a multiphysics simulation software this is unlikely.

Table 4.6 shows the RMS of the RC voltages and currents for different output resistances. At 1Ω the current and voltage is per definition equal. The result shows that a high output resistance should be used. However, in these simulations it is easier to use an open circuit, as this means the coupling between the magnetic fields and electrical circuit physics nodes is not required.

Figure 4.17 shows the measured RC voltage for different output resistances. The magnitude of the measurements are greatly affected by the resistance. Since the voltage output is the current reading it is very important to use a high output resistance to get an accurate result. The phase is not affected by the output resistance.

4.3 Summary and Discussions

Several tests are conducted in the laboratory rig, and using the FEM model. These tests are summarized, discussed and compared in this section.

4.3.1 Laboratory Tests

The laboratory tests are conducted with various conductor positions using a 32 A 50 Hz current output. The accuracy of the RC compared to the reference CT is 1.6% in the centered position. Adjustments are showing different results based on which direction they are done. Horizontal adjustments towards the discontinuity decreases the accuracy highly. When positioned to adjoin the RC insulation, the accuracy increases. The other direction the accuracy is not changed much, but decreases greatly when adjoined with the RC. The vertical adjustments show the same trend as the horizontal, but with smaller changes. This is likely due to the discontinuity not located exactly vertically centered, but somewhat towards the top as seen in figure 4.1. Diagonal adjustments show a clear trend when adjusted from the bottom left to top right, and the effect of the discontinuity is likely seen in the high error when adjusted towards the discontinuity. The other diagonal has a low error, but a less clear trend. All this indicates that the error of the RC is not readily estimated for different conductor positions. Likely this is highly due to the lack of roundness of the RC. Additionally, the discontinuity influences the results. It is also possible that the winding is not distributed equally around the coil.

Table 4.5: Output voltage RMS ratio to case with $\delta = 1°$ and composite error for $x, y = 0, 20$ mm conductor position for different discontinuities.

δ	RMS ratio to $\delta = 1°$	Comp. error of $x, y = 0, 20$ mm compared to centered position [%]
$-5°$	0.998	1.38
$0°$	1.012	4.37
$1°$	1	0.46
$10°$	0.975	2.73

Based on the results from the test conducted in the laboratory experiments it can be concluded that the error of the RC is quite high. This can however be explained by the RC used as it should be highly possible to design RCs with higher accuracy. It is reasonable to assume that RCs designed for protection applications would differ from those designed for use in less critical areas. It is also of importance that the reference CT has an error of $+1\%$, but results showed that during a 30 A the CT measured around 29.95 A which indicates that the error is negative or that the Omicron is not outputting 30 A. If the Omicron outputs less than 29.95 A it means the RC is more accurate than indicated in these tests. This makes it especially difficult to assess the integrity of the results.

Table 4.6: Output resistance and measured voltage and current in RC.

$R[\Omega]$	RMS voltage [μV]	RMS current [μA]
1	0.32	0.32
1000	57.80	0.06
$100k$	70.43	7.04e$-$4
∞	70.56	0

The test rig offers many possibilities for testing with the RC. Some adjustments to the test rig should however be considered. A proper way of locking the RC is lacking, which means that adjustments in the conductor position must be measured with a caliper to verify the position. This is a time consuming, and not very precise method. If the RC is locked in a precise position, then the horizontal adjustments can be done using the rulers without relying on caliper measurements to verify the position.The vertical adjustments are also difficult to set properly, as changing the height tends to change the angle as well. This is because the angle of the horizontal arm is not locked to the vertical arm. When unfastening the locking screw, the horizontal arm will be free to move both vertically and horizontally which in turn makes it hard to make vertical adjustments as the angle might not be equal for each adjustment. A solution which locks the angle while adjusting the vertical height

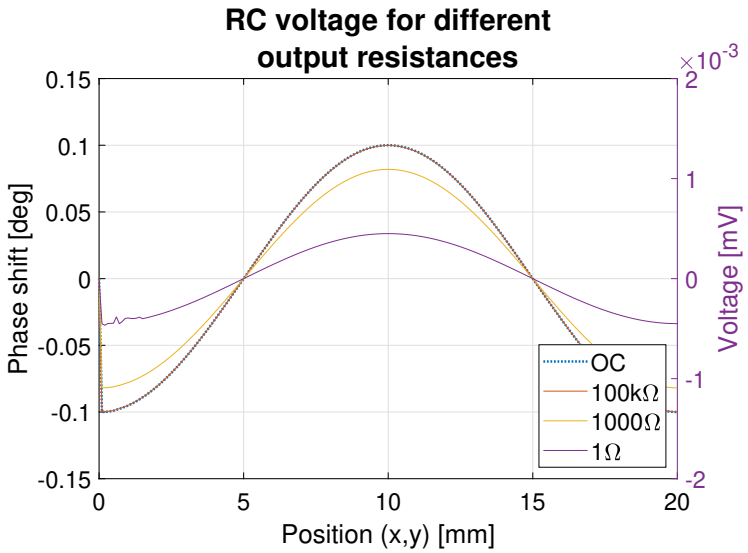

Figure 4.17: Measured RC voltage for different output resistances for a sample period. OC - open circuit, $100k\Omega$, and 1000Ω plotted on left axis, and 1Ω voltage plotted on right axis due to very low voltage output. The OC voltage and $100k\Omega$ overlaps and can be hard to distinguish.

will improve this. Because angle tests have not been performed as a part of this thesis, future tests should also include these. The tested RC should be as round as possible so that the results can be compared more efficiently with simulated results. Additionally the RC should be fastened to the rig in a manner which prevents any changes to its structure for the duration of the tests. Ideally, the frame is created to fit the exact shape of the RC.

The Omicron is able to output a relatively constant current level which is important for the accuracy of the results. Limited to 32 A due to the banana cables it is not well suited for the RC tested, which is rated at 200 A. At 32 A the RC is not performing at its designed level, which could lead to less performance, and the noise to current ratio is higher. According to the producer, the RC is supposed to have a accuracy of $\pm 1\%$, but in the tests the accuracy is actually around 1.6% which indicates that the current is too low.

4.3.2 Finite Element Method Modeling

Overall results from the simulations indicates that the model is properly adjusted in terms of induced voltages, magnetic fields and circuit operation. The conductor position simulations for the configuration with a low number of turns results in high overall composite errors compared to the laboratory tests. In these simulations positions furthest from the

centered position, ie. 83 mm and 58.7 mm results in a very high error compared to the other positions. The same tests conducted with a inhomogeneous winding distribution does not impact the results greatly in how the errors are randomised. The overall errors are greatly increased, but apart from the error dip at $x, y = 0, -83$ mm the winding distribution does not seem to explain the randomness in the laboratory results. Increasing the number of turns to 48 greatly impacts the magnitude of the errors. This results in composite error values resembling the laboratory tests. The horizontal adjustments now have the highest error when the conductor is positioned close to the discontinuity, which seems more reasonable compared to the horizontal adjustments for 16 turns. The phase shifts are significant, but overall less than $0.35°$. The discontinuity seems to make the RC lag the conductor current, as adjustments towards higher x-coordinates results in positive phase shifts. Simulations performed for different discontinuities are not clear, but seems to indicate that large discontinuities are not ideal. Simulations for output resistances shows that a high value for the output resistance is important, as even 1000Ω results in a large voltage drop, but simulating with an open circuit is the easiest method to implement, as it means the electric circuit physics node is not required.

The adjustments are likely a lot more influential when the turns number is low due to clearer differences between positions. With a high turns number, the local configuration of the coil at a specific position is more homogeneous, because more windings are present there. The simulation results resembles the laboratory results in terms of the the values of the composite error, and hence future models should be based on a high number of turns. A higher number of turns is not easy to implement, because the sweep function struggles to draw sharp turns. It is however, possible to simulate a lot of turns using a multiturn function on a solid block.

4.3.3 Common Discussions

The results from the laboratory and simulation tests shows quite different values, and are difficult to compare. The simulations performed with 16 turns results in composite errors much higher in magnitude compared to the laboratory results, but the 48 turns geometry lowers the error to a similar level. The errors measured in the laboratory tests does however vary greatly, and shows no clear trends.

It is not possible to design compensating techniques which are verified based on these measurements. For verifying compensating techniques the measurements must be similar, such that compensation techniques created in the software works for the real RC as well. It is possible that the RC used is not ideal for these tests. With a more refined laboratory

setup, and with a more suitable RC it is likely easier to find trends in the output which can be recreated in the FEM model. The lack of roundness of the RC tested is very difficult to simulate, which means rounder RCs should be used in testing. It is also possible to design compensating techniques purely based on the simulation results, but his is not guaranteed to work with real RCs.

Although the laboratory tests has not been able to verify the model the FEM shows promising prospects for the research on RCs. The geometry can be built quite advanced compared to lumped and mathematical models, and nonideal conditions can be applied such as temperature deviations, frequency deviations and transient currents. Integrators and compensation can be implemented in the model through COMSOL itself or through Simlink LiveLink for COMSOL which enables the benefits of signal processing in Simulink to be incorporated in the model. This means lots of reasearch topics can be investigated without the need for development of real microcontrollers for integration and compensation and the use of laboratory space.

Chapter 5

Conclusions & Further Work

In this thesis the accuracy of RCs is assessed. The work consists of both laboratory work and simulations. The thesis is concluded in the following bullet points:

- A laboratory setup is designed, and a commercial RC is tested under various conductor positions. The resulting output is difficult to evaluate due to lack of clear trends. The overall error in the RC is 1.6% and varies with up to 0.25 percentage points when the conductor position is adjusted of-center.
- A FEM model of a RC is created. The model is simulated for different parameters to verify the integrity of the model. Simulations are performed for eccentric conductor positions in three configurations: low number of turns, low number of inhomogeneously distributed turns and high number of turns. Low number of turns results in high errors, and the inhomogeneous winding distribution does not randomize the output similarly the laboratory tests. The high number of turns results in low errors, equal the magnitudes in the laboratory tests, and clear trends.
- The laboratory results are hard to evaluate but emphasizes the need for compensation for the RC. The laboratory results are also important for verifying the simulation model. The laboratory setup and the equipment is not sufficient to achieve the appropriate results.
- The FEM model is a suitable method to simulate the RC in a complex environment with possibilities for adjustments and extensions. The FEM model can be extended to include integrators and compensation techniques and can hence be used to test

these solutions in a controlled environment without need for extensive laboratory tests.

- Use of the model for research on the RC can improve the accuracy of the RC significantly by implementing compensation techniques and hence make it more appealing in interoperable differential protection schemes and reliable SPS operation.

5.1 Further Work

Several suggestions are presented for the future work on the thesis topics in the following list:

- The laboratory setup has several limitations which makes it challenging to make accurate measurements. Vertical adjustments should be tweaked such that the angle is held constant by utilizing a rectangular arm instead of a vertical arm. Ease of adjustments should be ensured by installing rulers to indicate the position.
- The RC frame is not custom built for the RC which means it is difficult to achieve the true centered conductor position. It is problematic to develop a frame for the RC used because of its lack of roundness. A round RC should be used and fitted to a custom-built frame which ensures a constant position and assured centered conductor position.
- The reference CT used has an error which adds uncertainty to the measurements. Future testing should either use the centered position as a reference or use a measuring device which has a very low or known error.
- The number of turns in the FEM model showed great improvement when increased to 48 turns. This is still a low number and hence the number of turns should be increased further. The current method of building the model does however prohibit this as the geometry gets to complex for the sweep function to properly build the thin wires. One suggested method is to use a multiturn function which uses a solid block of material and emulates a finite number of turns inside this block. Another method is to build the geometry in a CAD specific software. The geometry can then be imported to COMSOL and used in the physics environment.
- The FEM model is a simple RC which does not include an integrator. This means it does not read the conductor current. Future development can build on this model and focus on methods to determine the true error of the measurements compared to the actual conductor current. This requires an integrator. The integrator can be

developed in COMSOL, but the easiest method is likely to use COMSOL LiveLink for Simulink to integrate the FEM RC model in Simulink and build the integrator using blocks in Simulink. In Simulink it is also easy to implement compensation on the RC output which means some compensating techniques can be tested in a controlled environment.

- As laboratory results are inconsistent the FEM model has not been verified. Development on the model should make sure that the methods can be verified by comparing the results to a refined RC accuracy test or through the use of an integrator such that the output can be compared with the conductor current.

Bibliography

[1] D Karlsson, L Broski, and S Ganesan. Maximizing power system stability through wide area protection. In *57th Annual Conference for Protective Relay Engineers, 2004*, pages 403–418, 2004.

[2] A G Phadke, P Wall, L Ding, and V Terzija. Improving the performance of power system protection using wide area monitoring systems. *Journal of Modern Power Systems and Clean Energy*, 4(3):319–331, 2016.

[3] M Faheem, S B H Shah, R A Butt, B Raza, M Anwar, M W Ashraf, Md.A. Ngadi, and V C Gungor. Smart grid communication and information technologies in the perspective of Industry 4.0: Opportunities and challenges. *Computer Science Review*, 30:1–30, 2018.

[4] Temitope Raphael Ayodele, Adiasa Jimoh, Josial L Munda, and J T Agee. Challenges of grid integration of wind power on power system grid integrity: A review. *International Journal of Renewable Energy Research*, 2(4):6, 2012.

[5] Statnett SF, Fingrid Oyj, Energinet, and Affärsverket Svenska Kraftnät. Challenges and Opportunities for the Nordic Power System. Technical report, 2016.

[6] Frank Kienle and Christian De Schryver. 100% Green Computing At The Wrong Location?, 10 2012.

[7] A Muir and J Lopatto. Final report on the August 14, 2003 blackout in the United States and Canada : causes and recommendations. Technical report, Office of Electricity Delivery & Energy Reliability, Washinton DC, 2004.

[8] F Li, X Yan, Y Xie, Z Sang, and X Yuan. A Review of Cyber-Attack Methods in Cyber-Physical Power System. In *2019 IEEE 8th International Conference on Advanced Power System Automation and Protection (APAP)*, pages 1335–1339, 2019.

[9] Loi Lei Lai, Hao Tian Zhang, Chun Sing Lai, Fang Yuan Xu, and S Mishra. Investigation on July 2012 Indian blackout. In *2013 International Conference on Machine Learning and Cybernetics*, volume 01, pages 92–97, 2013.

[10] I M El-amin and N H Al-abbas. Saturation of Current Transformers and its Impact on Digital Overcurrent Relays. In *2006 IEEE/PES Transmission & Distribution Conference and Exposition: Latin America*, pages 1–6, 2006.

[11] J R Linders, C W Barnett, J W Chadwick, P R Drum, K J Khunkhun, W C Kotheimer, P A Kotos, D W Smaha, J W Walton, P B Winston, and S E Zocholl. Relay performance considerations with low-ratio CTs and high-fault currents. *IEEE Transactions on Industry Applications*, 31(2):392–404, 1995.

[12] T Zheng, T Huang, Y Ma, Z Zhang, and L Liu. Histogram-Based Method to Avoid Maloperation of Transformer Differential Protection Due to Current-Transformer Saturation Under External Faults. *IEEE Transactions on Power Delivery*, 33(2):610–619, 2018.

[13] Y.C. Kang, S.H. Ok, S.H. Kang, and P A Crossley. Design and evaluation of an algorithm for detecting current transformer saturation. *IEE Proceedings - Generation, Transmission and Distribution*, 151(1):27–35, 2004.

[14] A Bagheri, M Allahbakhshi, D Behi, and M Tajdinian. Utilizing Rogowski coil for saturation detection and compensation in iron core current transformer. In *2017 Iranian Conference on Electrical Engineering (ICEE)*, pages 1066–1071, 2017.

[15] L Kojovic. PCB Rogowski coils benefit relay protection. *IEEE Computer Applications in Power*, 15(3):50–53, 2002.

[16] S Wang, X Cao, and L Chen. Study of ECT based on Rogowski coil used in smart substation. In *2013 IEEE 7th International Power Engineering and Optimization Conference (PEOCO)*, pages 61–65, 2013.

[17] H Heine, P Guenther, and F Becker. New non-conventional instrument transformer (NCIT) - a future technology in gas insulated switchgear. In *2016 IEEE/PES Transmission and Distribution Conference and Exposition (T&D)*, pages 1–5, 2016.

[18] Lj A Kojovic. Comparative performance characteristics of current transformers and Rogowski coils used for protective relaying purposes. In *2007 IEEE Power Engineering Society General Meeting*, pages 1–6. IEEE, 2007.

[19] C Xianghu, Z Xiangjun, D Feng, and L Ling. Novel PCB sensor based on Rogowski coil for transmission lines fault detection. In *2009 IEEE Power & Energy Society General Meeting*, pages 1–4, 2009.

[20] Chen Qing, Li Hong-bin, Zhang Ming-ming, and Liu Yan-bin. Design and characteristics of two Rogowski coils based on printed circuit board. *IEEE Transactions on Instrumentation and Measurement*, 55(3):939–943, 2006.

[21] M Chiampi, G Crotti, and A Morando. Evaluation of Flexible Rogowski Coil Performances in Power Frequency Applications. *IEEE Transactions on Instrumentation and Measurement*, 60(3):854–862, 2011.

[22] A Mingotti, L Peretto, and R Tinarelli. Effects of Multiple Influence Quantities on Rogowski-Coil-Type Current Transformers. *IEEE Transactions on Instrumentation and Measurement*, 69(7):4827–4834, 2020.

[23] M H Samimi, A Mahari, M A Farahnakian, and H Mohseni. The Rogowski Coil Principles and Applications: A Review. *IEEE Sensors Journal*, 15(2):651–658, 2015.

[24] A Mingotti, L Peretto, and R Tinarelli. A Simple Modelling Procedure of Rogowski Coil for Power Systems Applications. In *2019 IEEE 10th International Workshop on Applied Measurements for Power Systems (AMPS)*, pages 1–5, 2019.

[25] Gabriella Crotti, Domenico Giordano, and A Morando. Analysis of Rogowski coil behavior under non ideal measurement conditions.

[26] R Oganyan, N Gorbatenko, and M Lankin. Development of a mathematical model for determining the EMF of the secondary winding of a measuring current transformer based on the Rogowski coil. *IOP Conference Series: Materials Science and Engineering*, 680:12032, 2019.

[27] E Farjah, H Givi, and T Ghanbari. Application of an Efficient Rogowski Coil Sensor for Switch Fault Diagnosis and Capacitor ESR Monitoring in Nonisolated Single-Switch DC–DC Converters. *IEEE Transactions on Power Electronics*, 32(2):1442–1456, 2017.

[28] Tamás Orosz, Zoltán Ádám Tamus, and István Vajda. Modeling the high frequency behavior of the Rogowski-coil passive L/r integrator current transducer with analytical and finite element method. In *2014 49th International Universities Power Engineering Conference (UPEC)*, pages 1–4, 2014.

[29] Joachim Bertsch, Cedric Carnal, D Karlson, John McDaniel, and Khoi Vu. Wide-area protection and power system utilization. *Proceedings of the IEEE*, 93(5):997–1003, 2005.

[30] M R D Zadeh, T S Sidhu, and A Klimek. Implementation and Testing of Directional Comparison Bus Protection Based on IEC61850 Process Bus. *IEEE Transactions on Power Delivery*, 26(3):1530–1537, 2011.

[31] M C Janssen and A Apostolov. IEC 61850 impact on substation design. In *2008 IEEE/PES Transmission and Distribution Conference and Exposition*, pages 1–7, 2008.

[32] Mitalkumar Kanabar. Investigating performance and reliability of process bus networks for digital protective relaying. 2011.

[33] A Apostolov and D Tholomier. Impact of IEC 61850 on Power System Protection. In *2006 IEEE PES Power Systems Conference and Exposition*, pages 1053–1058, 2006.

[34] Q Huang, S Jing, J Li, D Cai, J Wu, and W Zhen. Smart Substation: State of the Art and Future Development. *IEEE Transactions on Power Delivery*, 32(2):1098–1105, 2017.

[35] R E Mackiewicz. Overview of IEC 61850 and Benefits. In *2006 IEEE PES Power Systems Conference and Exposition*, pages 623–630, 2006.

[36] T S Sidhu and P K Gangadharan. Control and automation of power system substation using IEC61850 communication. In *Proceedings of 2005 IEEE Conference on Control Applications, 2005. CCA 2005.*, pages 1331–1336, 2005.

[37] Salman Mohagheghi, J Stoupis, and Z Wang. *Communication Protocols and Networks for Power Systems – Current Status and Future Trends*. 4 2009.

[38] R Aguilar and J Ariza. Testing and configuration of IEC 61850 multivendor protection schemes. In *IEEE PES T&D 2010*, pages 1–8, 2010.

[39] Yuan. Yubo, Ji-Lei. Yi, and Yi. Yang. *IEC 61850-Based Smart Substation : Principles, Testing, Operation and Maintenance.* 2019.

[40] A Hakala-Ranta, O Rintamaki, and J Starck. Utilizing possibilities of IEC 61850 and goose. In *CIRED 2009 - 20th International Conference and Exhibition on Electricity Distribution - Part 1*, pages 1–4, 2009.

[41] V R Vinnakota, M Ziwen Yao, and D Atanackovic. Modelling issues of system protection schemes in energy management systems. In *2008 IEEE Canada Electric Power Conference*, pages 1–6, 2008.

[42] Daniel Duckwitz. *Power System Inertia*. PhD thesis, University of Kassel, 2019.

[43] J D McCalley and Weihui Fu. Reliability of special protection systems. *IEEE Transactions on Power Systems*, 14(4):1400–1406, 1999.

[44] James Mccalley, Oluwaseyi Olatujoye, Venkat Krishnan, Renchang Dai, Chanan Singh, and Kai Jiang. System Protection Schemes: Limitations, Risks, and Management, 2010.

[45] Peter Crossley, Franc Ilar, and D Karlsson. System protection schemes in power networks: existing installations and ideas for future development. *IET Conference Proceedings*, pages 450–453, 1 2001.

[46] M Begovic, D Novosel, D Karlsson, C Henville, and G Michel. Wide-Area Protection and Emergency Control. *Proceedings of the IEEE*, 93(5):876–891, 2005.

[47] Mohammad Reza Aghamohammadi, Sina Hashemi, and A Hasanzadeh. A new approach for mitigating blackout risk by blocking minimum critical distance relays. *International Journal of Electrical Power & Energy Systems*, 75:162–172, 2016.

[48] J Wang, B Huang, Y Li, and W Zhang. An optimized design of substation-area protection in smart substation. In *2017 IEEE 3rd Information Technology and Mechatronics Engineering Conference (ITOEC)*, pages 167–171, 2017.

[49] Amin Shotorbani, Sajad Madadi, and Behnam Mohammadi-ivatloo. Wide-Area Measurement, Monitoring and Control: PMU-Based Distributed Wide-Area Damping Control Design Based on Heuristic Optimisation Using DIgSILENT PowerFactory. In *Green Energy and Technology*, pages 211–240. 2018.

[50] T C Njenda, M E H Golshan, and H H Alhelou. WAMS Based Intelligent Under Frequency Load Shedding Considering Online Disturbance Estimation. In *2018 Smart Grid Conference (SGC)*, pages 1–5, 2018.

[51] R Hooshmand and M Moazzami. Optimal design of adaptive under frequency load shedding using artificial neural networks in isolated power system. *International Journal of Electrical Power & Energy Systems*, 42(1):220–228, 2012.

[52] M Moazzami and A khodabakhshian. A new optimal adaptive under frequency load shedding Using Artificial Neural Networks. In *2010 18th Iranian Conference on Electrical Engineering*, pages 824–829, 2010.

[53] S K Tso, T X Zhu, Q Y Zeng, and K L Lo. Investigation of extended fuzzy reasoning and neural classification for load-shedding prediction to prevent voltage instability. *Electric Power Systems Research*, 43(2):81–87, 1997.

[54] J A Laghari, H Mokhlis, A H A Bakar, and Hasmaini Mohamad. Application of computational intelligence techniques for load shedding in power systems: A review. *Energy Conversion and Management*, 75:130–140, 2013.

[55] Alstorm. *Network Protection & Automation Guide*. Alstorm Grid, 2011.

[56] Arun G. Horowitz, Stanley H.; Phadke. *Power System Relaying 4th edition*. John Wiley and Sons Ltd, 2014.

[57] E Vazquez, I I Mijares, O L Chacon, and A Conde. Transformer differential protection using principal component analysis. In *2006 IEEE Power Engineering Society General Meeting*, page 6 pp., 2006.

[58] NTNU. *Power system protection and control in digital substations, Research Project*. Accessed: June 1st 2021. [Online]. Available: https://www.ntnu.edu/prodig/power-system-protection-and-control-in-digital-substations.

[59] W Rogowski and W Steinhaus. Die Messung der magnetischen Spannung. *Archiv für Elektrotechnik*, 1(4):141–150, 1912.

[60] G M Hashmi, M Lehtonen, and M Nordman. Modeling and experimental verification of on-line PD detection in MV covered-conductor overhead networks. *IEEE Transactions on Dielectrics and Electrical Insulation*, 17(1):167–180, 2010.

[61] Ljumbomir a. Kojovic and Robert Beresh. Practical Aspects of Rogowski Coil Applications to Relaying. *IEEE PSRC Special Report*, (September):1–72, 2010.

[62] Yi Liu, Fuchang Lin, Qin Zhang, and Heqing Zhong. Design and construction of a Rogowski coil for measuring wide pulsed current. *IEEE Sensors Journal*, 11(1):123–130, 2010.

[63] J P Dupraz, A Fanget, W Grieshaber, and G F Montillet. Rogowski Coil: Exceptional Current Measurement Tool For Almost Any Application. In *2007 IEEE Power Engineering Society General Meeting*, pages 1–8, 2007.

[64] Zhenhua Li, Xin Xiang, Tinghe Hu, Ahmed Abu-Siada, Zhenxing Li, and Yanchun Xu. An improved digital integral algorithm to enhance the measurement accuracy of Rogowski coil-based electronic transformers. *International Journal of Electrical Power & Energy Systems*, 118:105806, 2020.

[65] X Zhang and L Mu. Design for digital integrator of Rogowski coil based on pipeline structure. In *2010 Asia-Pacific Power and Energy Engineering Conference*, pages 1–4, 2010.

[66] E Hemmati and S M Shahrtash. Digital Compensation of Rogowski Coil's Output Voltage. *IEEE Transactions on Instrumentation and Measurement*, 62(1):71–82, 2013.

[67] A Marinescu and I Dumbravă. Validation of the software for digital processing of a Rogowski coil output signal. In *2012 13th International Conference on Optimization of Electrical and Electronic Equipment (OPTIM)*, pages 1189–1192, 2012.

[68] B N Biswas, S Chatterjee, S P Mukherjee, and S Pal. A discussion on euler method: A review. *Electronic Journal Of Mathematical Analysis And Applications*, 1(2):294–317, 2013.

[69] L Ferkovic, D Ilic, and R Malaric. Mutual Inductance of a Precise Rogowski Coil in Dependence of the Position of Primary Conductor. *IEEE Transactions on Instrumentation and Measurement*, 58(1):122–128, 2009.

[70] L Ferkovic and D Ilic. Dependence of mutual inductance of a precise Rogowski coil on the primary conductor position. In *Proc. 15th IMEKO TC 4*, 2007.

[71] E . Suomalainen and J Hällström. Uncertainty estimate of a split-core Rogowski coil for high AC current. In *CPEM 2010*, pages 653–654, 2010.

[72] *Instrument transformers – Part 9: Digital interface for instrument transformers*. IEC 61869-9:2016, Standard Norge. [Online]. Available: https://www.standard.no/no/Nettbutikk/produktkatalogen/Produktpresentasjon/?ProductID=822000.

[73] Precisionfiberproducts.com. *Fluke i2000 Flex AC Current Clamp, 2000A*. Accessed: May 24th 2021 [Online]. Available: https://precisionfiberproducts.com/fluke-i2000-flex-ac-current-clamp-2000a/.

[74] Fluke. *i3000s/i2000 Flex AC Current Proble Instruction Sheet*. Accessed: May 27th 2021 [Online]. Available: https://dam-assets.fluke.com/s3fs-public/i3000s__iseng0100.pdf.

[75] Pearson Electronics Inc. *PEARSON™ CURRENT MONITOR MODEL 110*. Accessed: June 7th 2021 [Online]. Available: https://www.pearsonelectronics.com/pdf/110.pdf.

Appendix A

Laboratory Tests Supplements

This appendix includes materials relevant for the laboratory tests.

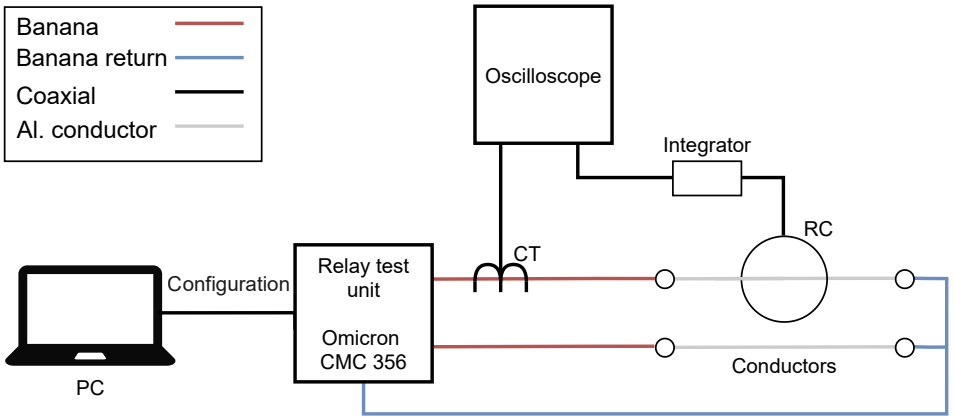

Figure A.1: Schematic of the RC accuracy test setup. The schematic shows the connections, devices and the cable types in the setup.

A.1 Additional Laboratory Setup Photographs

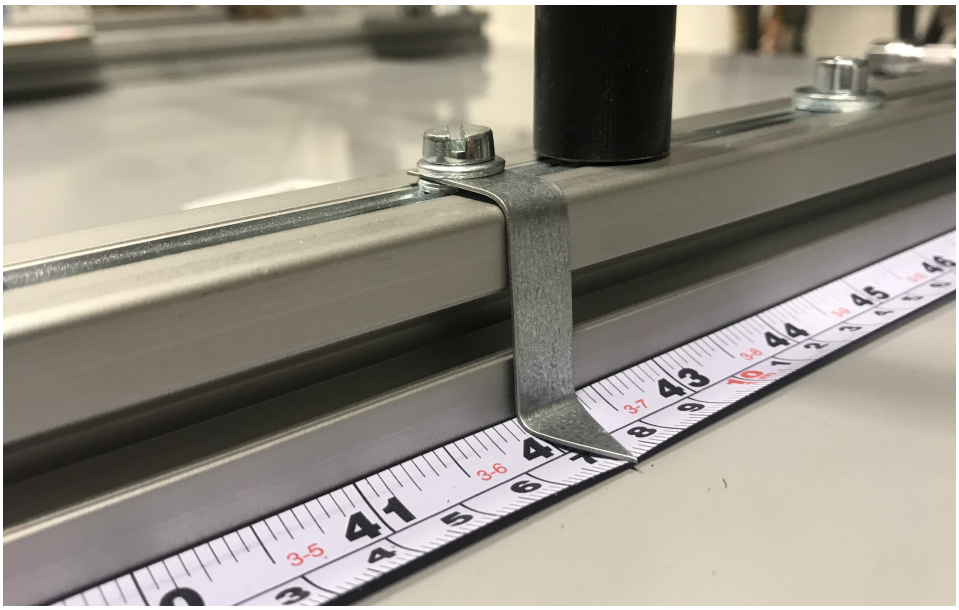

Figure A.2: Horizontal adjustment in the test rig. The ruler is used to show the placement of the conductor and is indicated by the arrow. The black vertical cylinder in the background is the conductor stand. Adjustments are done by unscrewing the bolt in the top right of the photo.

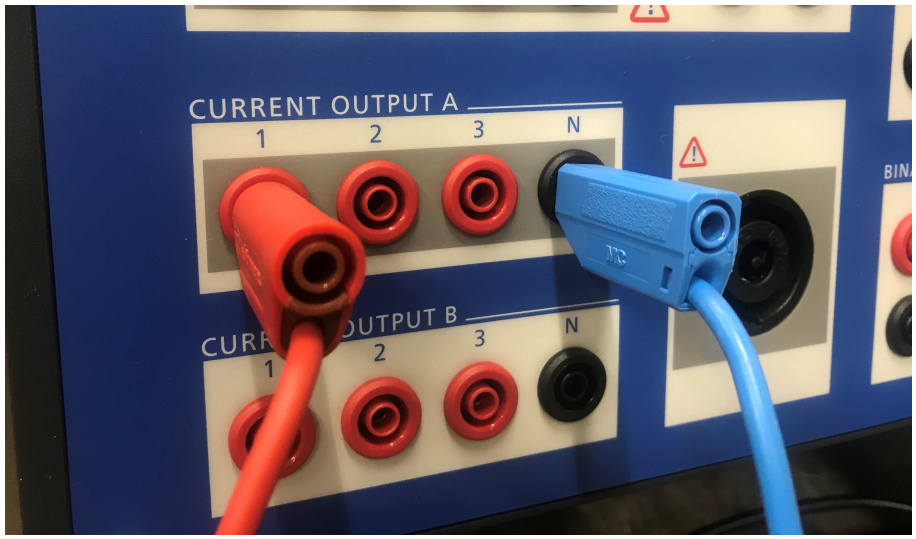

Figure A.3: Connection of the terminals to the Omicron current output using banana plugs. The current is outputted through current output A terminal one and returned on the neutral terminal. The schematic in figure A.1 uses the same color scheme, but the external conductor (bottom) is not connected.

Figure A.4: The banana plug connected to the aluminium conductor with the RC in the background.

Figure A.5: Closeup of the RC discontinuity. The locking mechanism is located just above the strip.

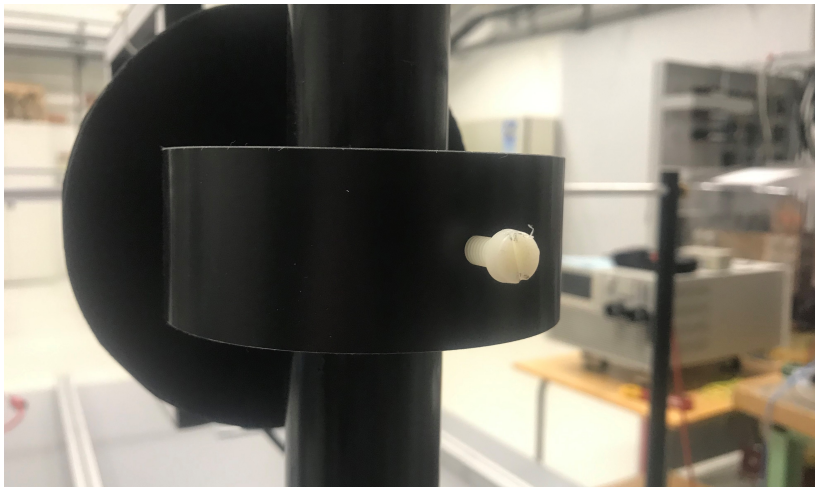

Figure A.6: The vertical adjustment of the conductor position. Unscrewing the screw enables vertical adjustment of the frame. Since the frame is held up by the cylindrical arm, it means the angle of the frame is also adjustable, which makes it difficult to make proper vertical adjustments with no other parameter changes.

Figure A.7: Protractors for adjustment of conductor angle. Arrow indicator indicates the angle.

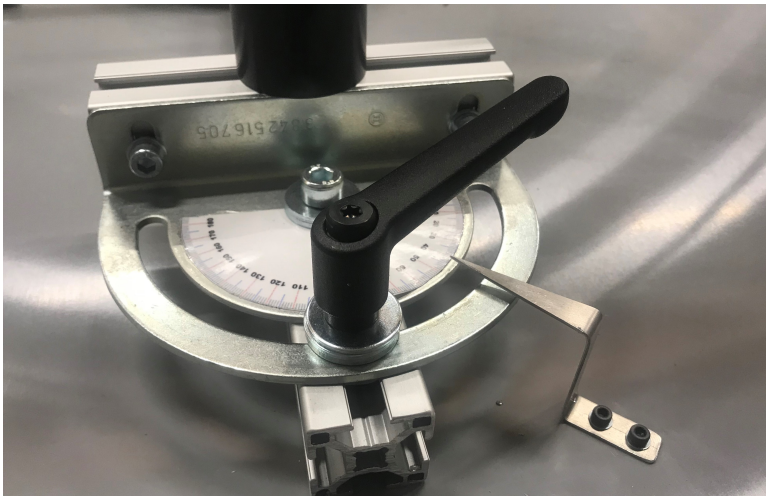

Figure A.8: Adjustment of angle of lower cylindrical arm for adjustment of both conductor position and angle simultaneously.

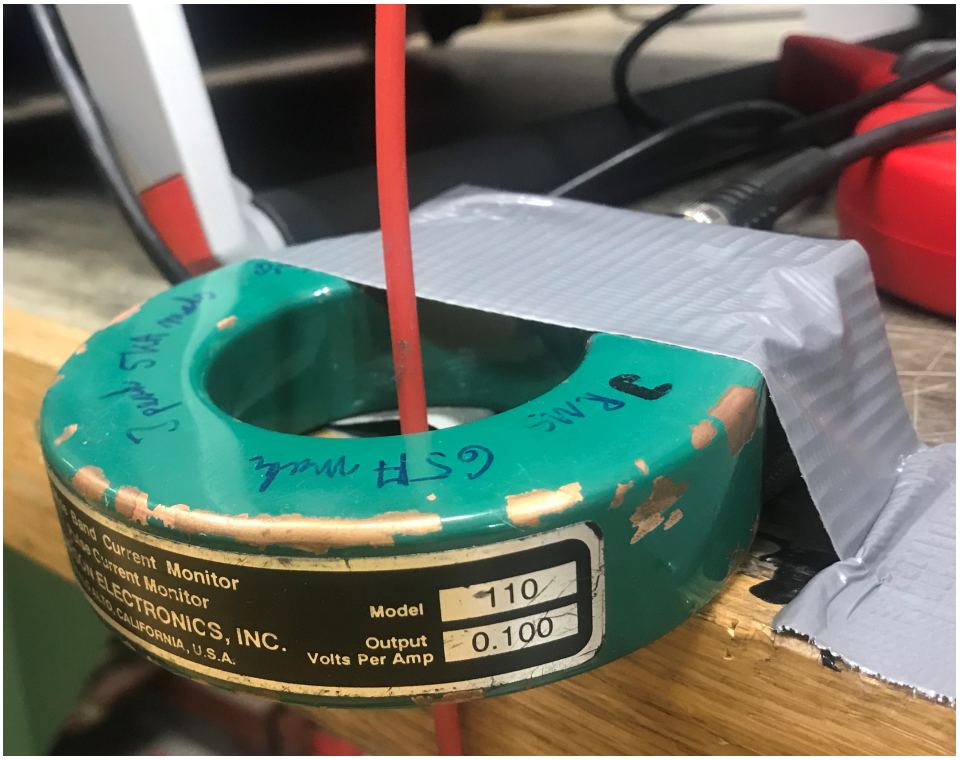

Figure A.9: Reference Pearson Electronics inc. current monitor used for comparisons with the RC. It measures the output of the Omicron.

A.2 Tests with ITECH Current Generator

An ITECH was also set up to test the setup at higher currents as the ITECH with a transformer is able to output currents up to 100 A. The setup was connected similarly to the Omicron setup, but installed with thicker cables as shown in figure A.10 in order to protect against overheating.

Figure A.10: Cables from ITECH connected to conductors on test rig.

Testing the RC using high currents have several benefits: Firstly the amplitude to noise ratio becomes smaller, decreasing the impact of the noise. Secondly the currents are closer to the rated value of the RC at 200 A which means the RC is running at levels closer to its design value.

During the tests it is observed that the CT is not measuring a constant current of 100 A. The current is hence measured for see the effect over time. Figure A.11 shows how the current of the ITECH drops of with different current levels over time. The figure shows that at 67 A and 100 A the drop off is high, which results in difficult comparisons. It also indicates that the noise is significantly less at 100 A.

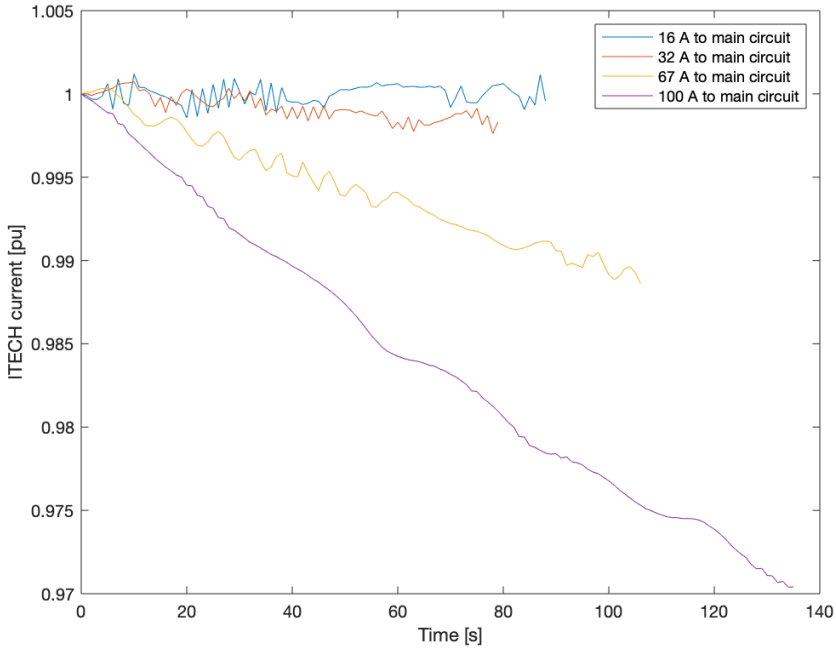

Figure A.11: Per unit current output of ITECH over time for different output levels.

The reason behind the current drop is not thoroughly investigated. It is however theorized that as the conductors are heated, at a constant voltage level the ITECH does not require the same current, and can hence reduce it over time. Due to the current drop off, the ITECH is not suited for testing the accuracy of the RC. The ITECH proves to be insufficient due to its current drop over time which makes it difficult to properly compare tests.

Appendix B

Finite Element Method Simulations Supplements

This appendix contains supplementary material and figures for the simulation tests.

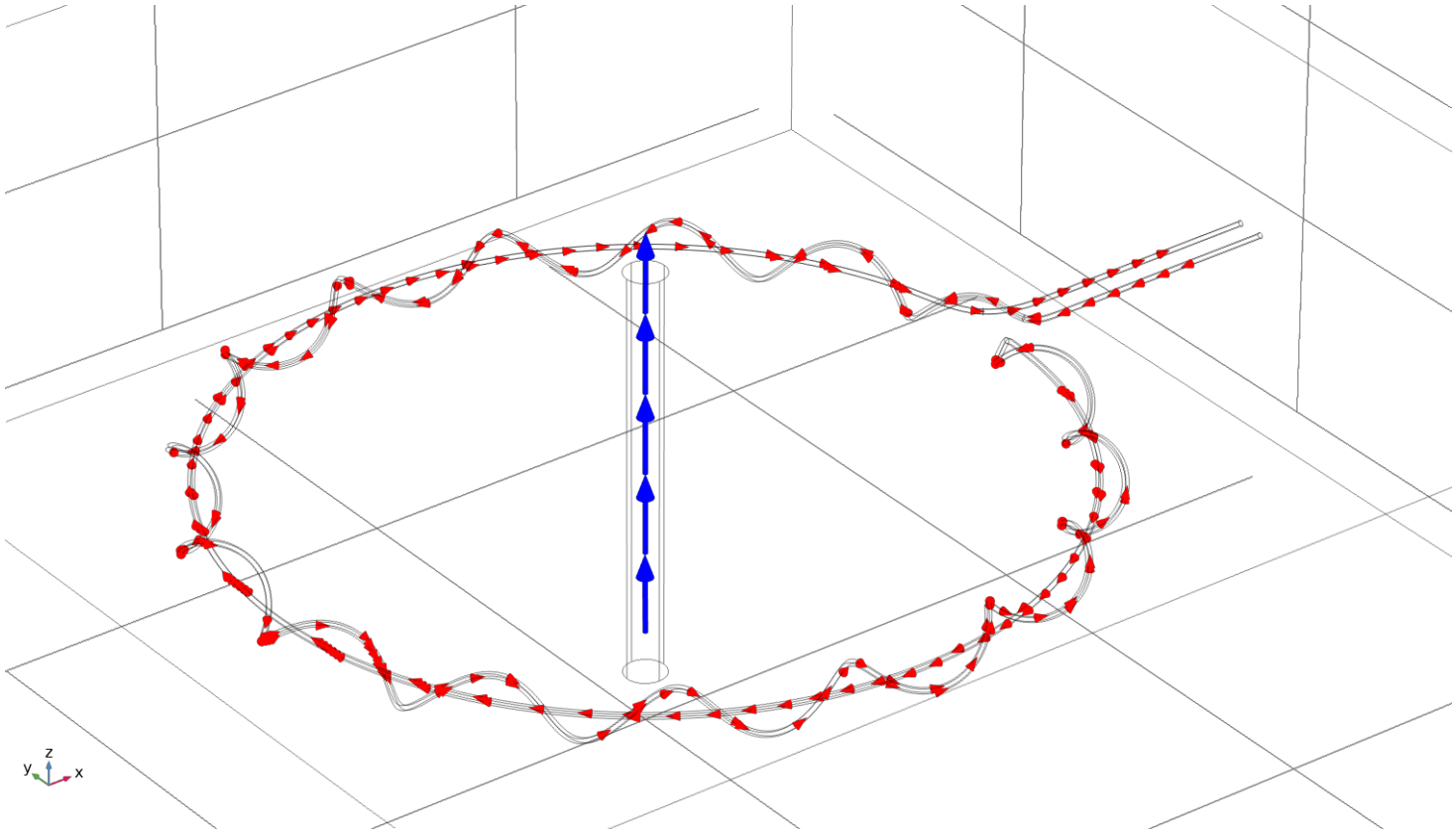

Figure B.1: Direction of numerical calculated wire in conductor (blue) and RC (red) indicated by arrowheads after the initial coil geometry analysis. If the initial coil geometry analysis fails, the current directions does not follow the coil windings.

Table B.1: X- and y-coordinates for different conductor positions in a parametric sweep simulation.

Test number	x-coordinate [mm]	y-coordinate [mm]	Test type
1	0	0	Reference
2	0	20	Horizontal
3	0	40	Horizontal
4	0	60	Horizontal
5	0	83	Horizontal
6	0	-20	Horizontal
7	0	-40	Horizontal
8	0	-60	Horizontal
9	0	-83	Horizontal
10	20	0	Vertical
11	40	0	Vertical
12	60	0	Vertical
13	83	0	Vertical
14	-20	0	Vertical
15	-40	0	Vertical
16	-60	0	Vertical
17	-83	0	Vertical
18	20	20	Diagonal
19	40	40	Diagonal
20	58.7	58.7	Diagonal
21	20	-20	Diagonal
22	40	-40	Diagonal
23	58.7	-58.7	Diagonal
24	-20	-20	Diagonal
25	-40	-40	Diagonal
26	-58.7	-58.7	Diagonal
27	-20	20	Diagonal
28	-40	40	Diagonal
29	-58.7	58.7	Diagonal

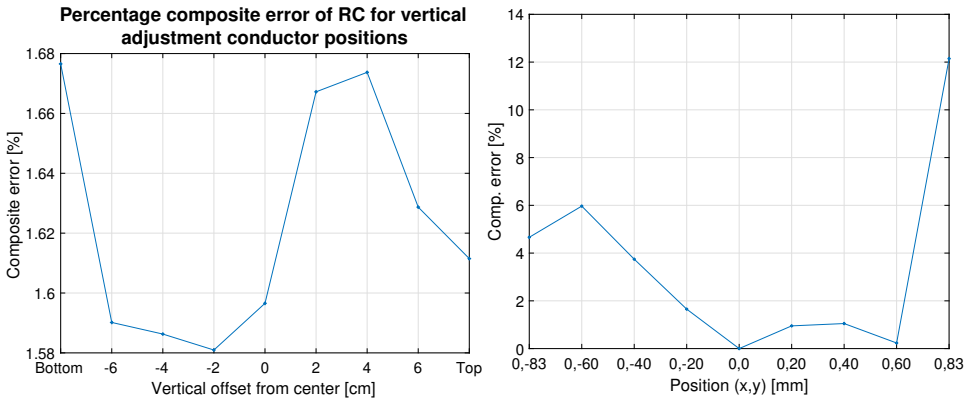

(a) Laboratory results

(b) Simulation results

Figure B.2: A comparison of the vertical adjustments of the conductor position in the laboratory tests, and the simulations with an inhomogeneous winding distribution.

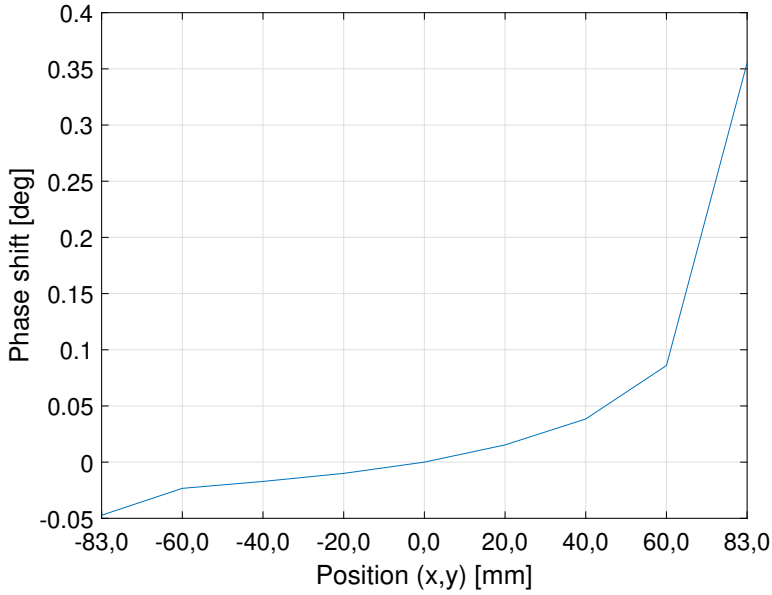

Figure B.3: Phase shift from different conductor positions when adjusted horizontally. Homogeneous winding distribution with 48 turns.

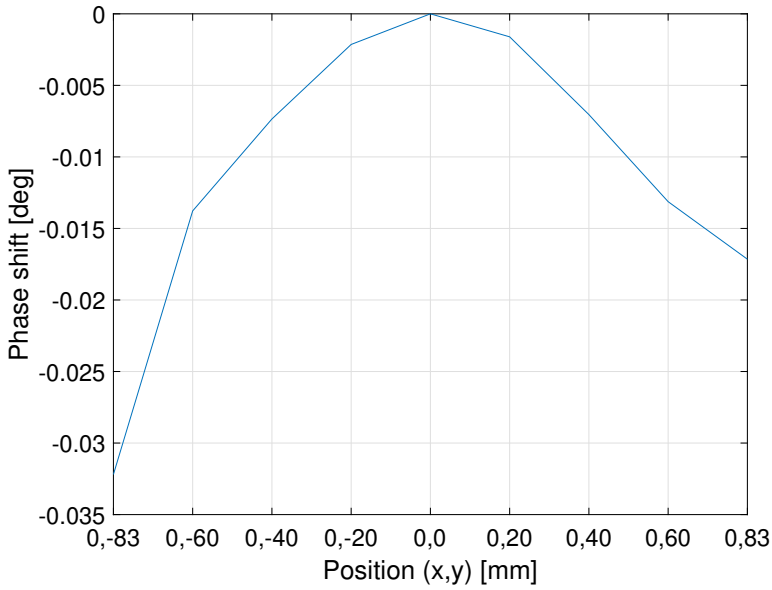

Figure B.4: Phase shift from different conductor positions when adjusted vertically. Homogeneous winding distribution with 48 turns.

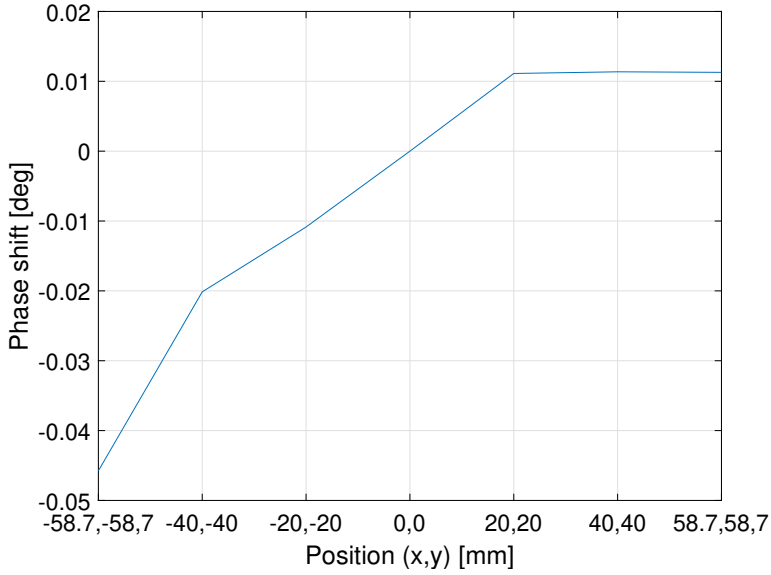

Figure B.5: Phase shift from different conductor positions when adjusted diagonally. Homogeneous winding distribution with 48 turns.

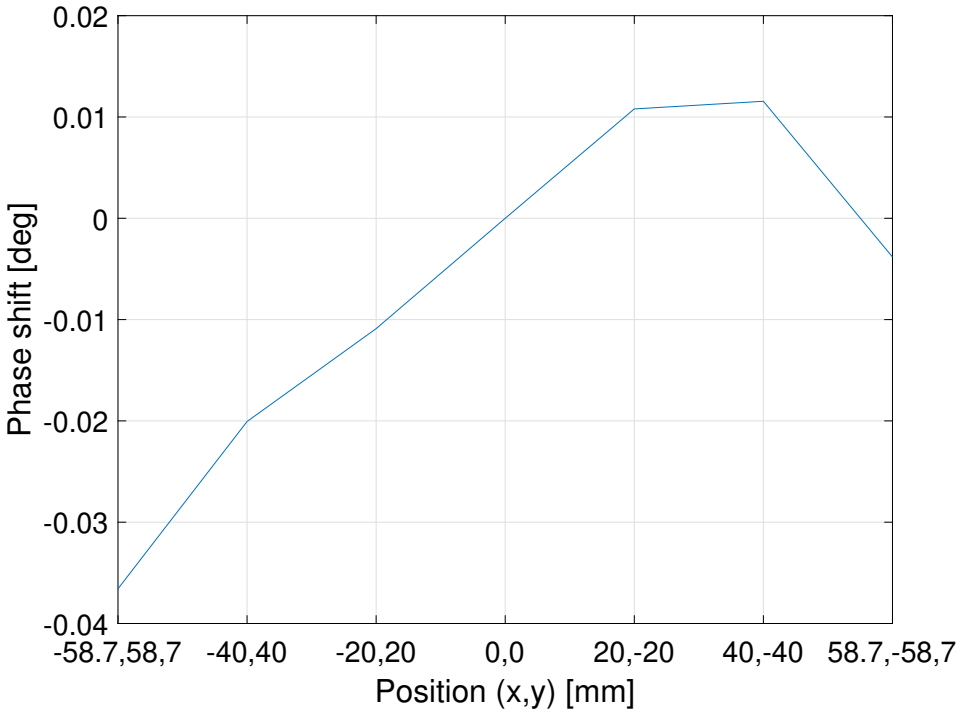

Figure B.6: Phase shift from different conductor positions when adjusted diagonally. Homogeneous winding distribution with 48 turns.

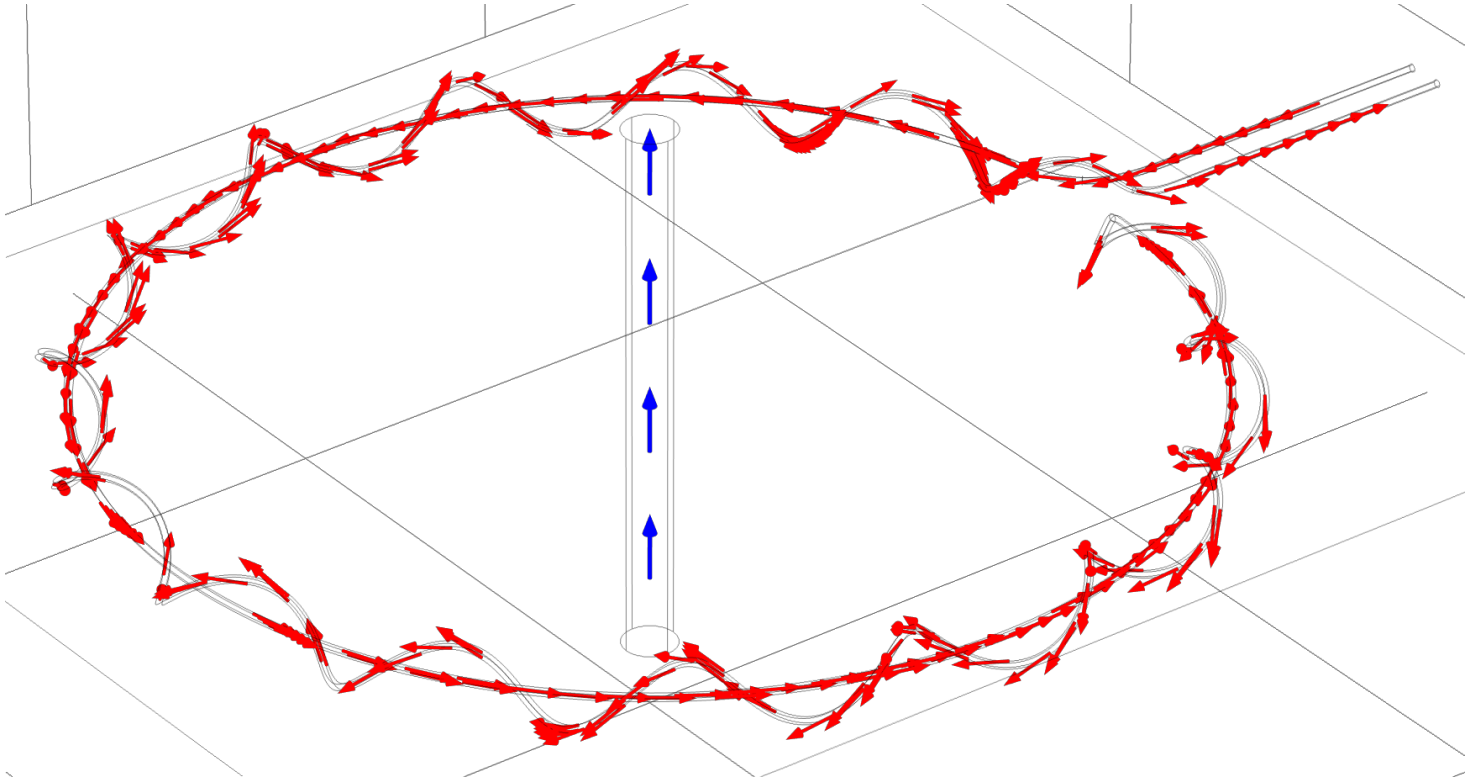

Figure B.7: Current density in the coil indicated by red arrows and in the conductor indicated by blue arrows. current direction is directed into the return wire, and then through the windings. 1Ω output resistance and $\delta = 1°$.

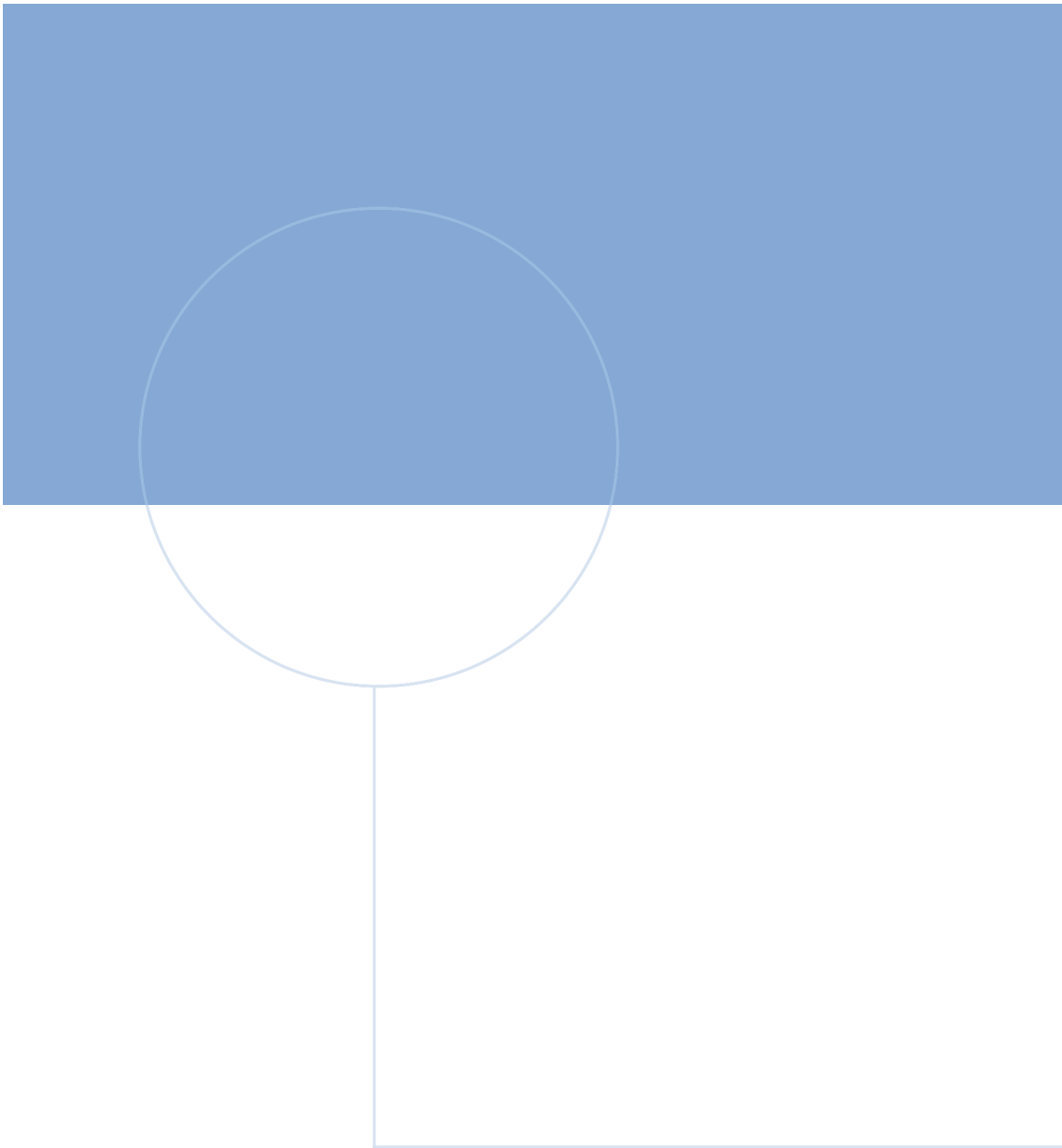

NTNU

Norwegian University of
Science and Technology